THE LATE- TO POST-CALEDONIAN EXTENSIONAL HISTORY OF NORTHWEST HINNØY, NORTH NORWAY

Stephanie M. Mager

A Thesis

Submitted to

the Graduate Faculty of

Auburn University

in Partial Fulfillment of the

Requirements for the

Degree of

Master of Science

Auburn, Alabama
August 8, 2005

THE LATE- TO POST-CALEDONIAN EXTENSIONAL HISTORY OF NORTHWEST HINNØY, NORTH NORWAY

Stephanie M. Mager

Stephanie M. Mager

5/2/05
date

Copy sent to:

Name Date

VITA

Stephanie Marie Mager, daughter of Stephen Edward and Jeanne Eleanor (Payette) Mager, was born September 16, 1978, in Fitchburg, Massachusetts. She graduated from Courtland High School in Spotsylvania, Virginia, in 1996. She attended the College of William and Mary in Williamsburg, Virginia, and graduated with a Bachelor of Science with concentrations in Geology and Mathematics in May, 2000. She entered Graduate School at Auburn University in August, 2000, where she studied Structural Geology under Dr. Mark G. Steltenpohl.

THESIS ABSTRACT

THE LATE- TO POST-CALEDONIAN EXTENSIONAL HISTORY OF NORTHWEST HINNØY, NORTH NORWAY

Stephanie M. Mager
Master of Science, August 8, 2005
(B. S., College of William and Mary, 2000)

100 typed pages

Directed by Mark G. Steltenpohl

This investigation focuses on the lithologies and late- to post-Caledonian, upper crustal structures exposed in westernmost Hinnøy, north Norway, and the information about the timing and kinematics of faults that they may yield. The main objective is the mapping of brittle to semi-brittle faults and determining what significance they have for Caledonian and later tectonic evolution of rocks in the region.

Two major lithologies are found in the study area, migmatitic gneiss and mangerite, along with an intrusive dolerite and many pseudotachylites. The major rock types have been metamorphosed to granulite facies in the southern part of the study area and to amphibolite facies in the northern part.

Important structural features of the study area includes many shear zones and eight major brittle faults. The shear zones are defined by cataclasites, mylonites, and ultramylonites and demonstrate semi-brittle to plastic behavior. They appear to occur in two sets over the study area. One set has a northeast strike, the other a northwest strike. The northeast-striking set appears to have formed first and demonstrates oblique-dextral reverse movement. The younger, northwest-striking set demonstrates oblique-sinistral normal movement. The brittle faults observed have a major plane along which brittle deformation and displacement has occurred. Analysis of data collected along these faults implies that general movement along faults striking northeast was oblique-sinistral normal and movement along the northwest-striking faults was oblique-dextral normal.

Eight samples were selected for $^{40}Ar/^{39}Ar$ isotopic analysis using both muscovite and potassium feldspar. The muscovite analysis provided a general cooling history beginning sometime after ca. 570 Ma and before ca. 440 Ma. The potassium feldspar results document a pulse, or multiple pulses, of uplift and cooling between ca. 235 Ma and 185 Ma.

Structures in the study area are related to a structural anomaly that is not yet completely understood. Several structural anomalies have been previously documented for this area: 1) a Jurassic basin postulated by Davidsen and others (2001); 2) Heier's zone of pseudotachylite (Heier, 1960); 3) the Eidsfjord fault; and 4) an extensional detachment postulated by Steltenpohl and others. Results of this study lend at least some support for all of these anomalies, implying that they are most likely related to one another.

The style manual used for this manuscript is the manual provided by the United States Geological Survey. Software used in the production of this manuscript is Microsoft Office©, Canvas 7™ , and StereonetPPC 6.0©.

ACKNOWLEDGEMENTS

The author would like to thank Dr. Arild Andresen for his many contributions and assistance with the field work, and her teammates and friends for their incredible moral support.

TABLE OF CONTENTS

LIST OF FIGURES

INTRODUCTION

This investigation focuses on the lithologies and late- to post-Caledonian (i.e., post-mid-Devonian), upper-crustal structures exposed in westernmost Hinnøy, north Norway (Figure 1). Post-Caledonian structures in this area may yield important information about the kinematics and timing of faults that otherwise can only be inferred from geophysical studies of offshore basin-bounding structures. Previous work in western Hinnøy has indicated the presence of brittle extensional structures and thrusts (Heier, 1960; Løseth and Tveten, 1996; Markl and Bucher, 1997; Olesen et al., 1997; Klein et al., 1999; Steltenpohl et al., 2004), but little to no geometric, kinematic, or timing information has been presented about them.

Heier (1960) reported an extensive zone of pseudotachylites in an area now known as Heier's Zone of Pseudotachylites. Pseudotachylites are dark gray to black rocks that typically occur in irregular branching veins. They are often produced in the compression and shear associated with rapid and intense fault movements that generate seismic (i.e., earthquake) energy. Some pseudotachylites can behave like an intrusive with no structures obviously related to faulting (Bates and Jackson, 1987). Løseth and Tveten (1996) show the known extent of Heier's Zone (Figure 2). However, this zone has not yet been definitely related to any particular process, structure or deformation event.

The goal of this project is the mapping of brittle to semi-brittle faults on western Hinnøy and determining what significance they have for Caledonian and later tectonic evolution of rocks in the region. The specific objectives are 1) to produce a lithologic and structural map of the area, 2) to characterize the lithologies, and 3) to determine the timing and kinematics of structural features and crustal conditions of the deformation events that formed them, particularly the late-stage brittle extensional faults.

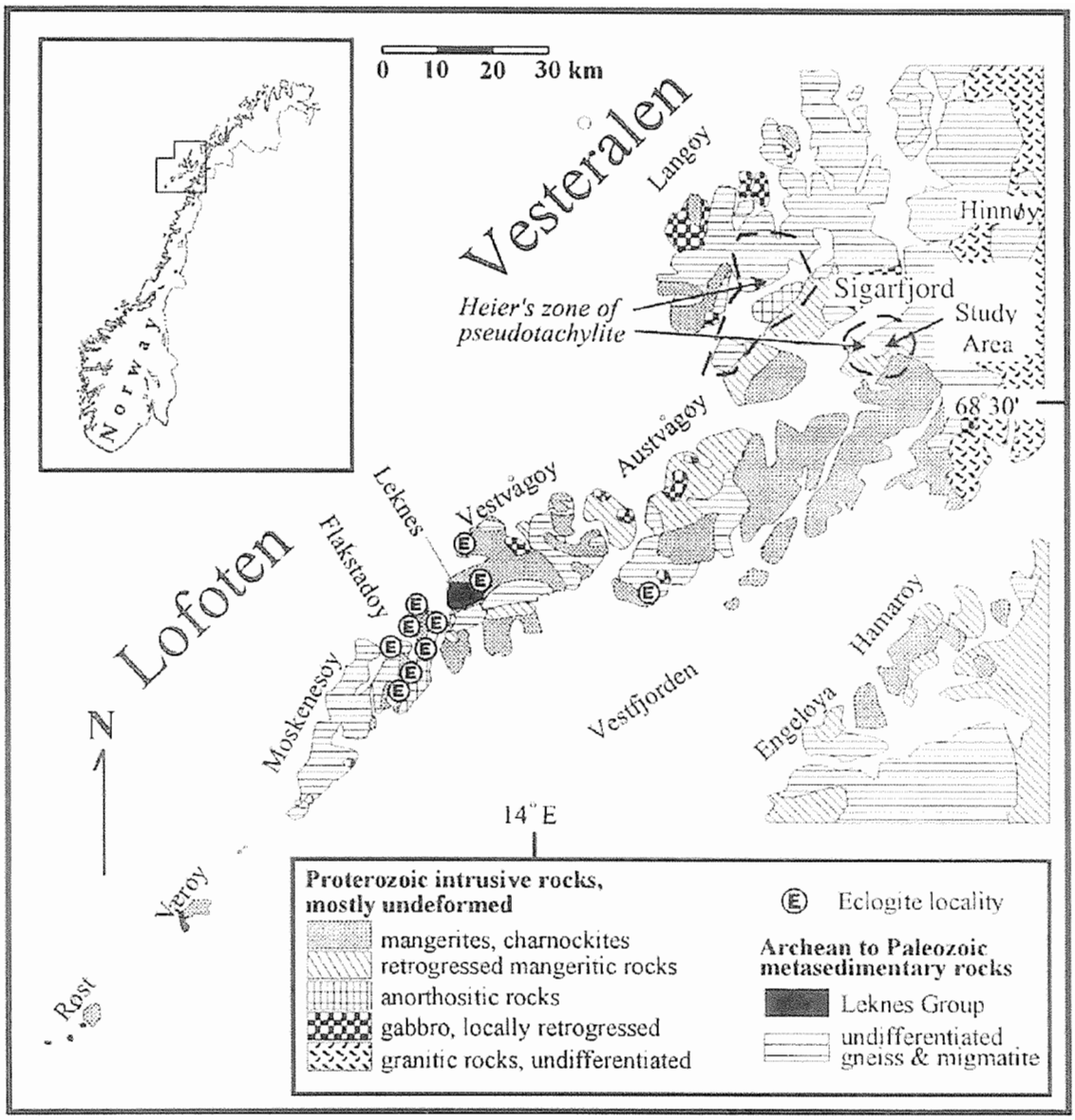

Figure 1: Location and general geology of study area (after Heier, 1960; Griffin et al., 1978; Markl and Bucher, 1997; Sigmond et al., 1984).

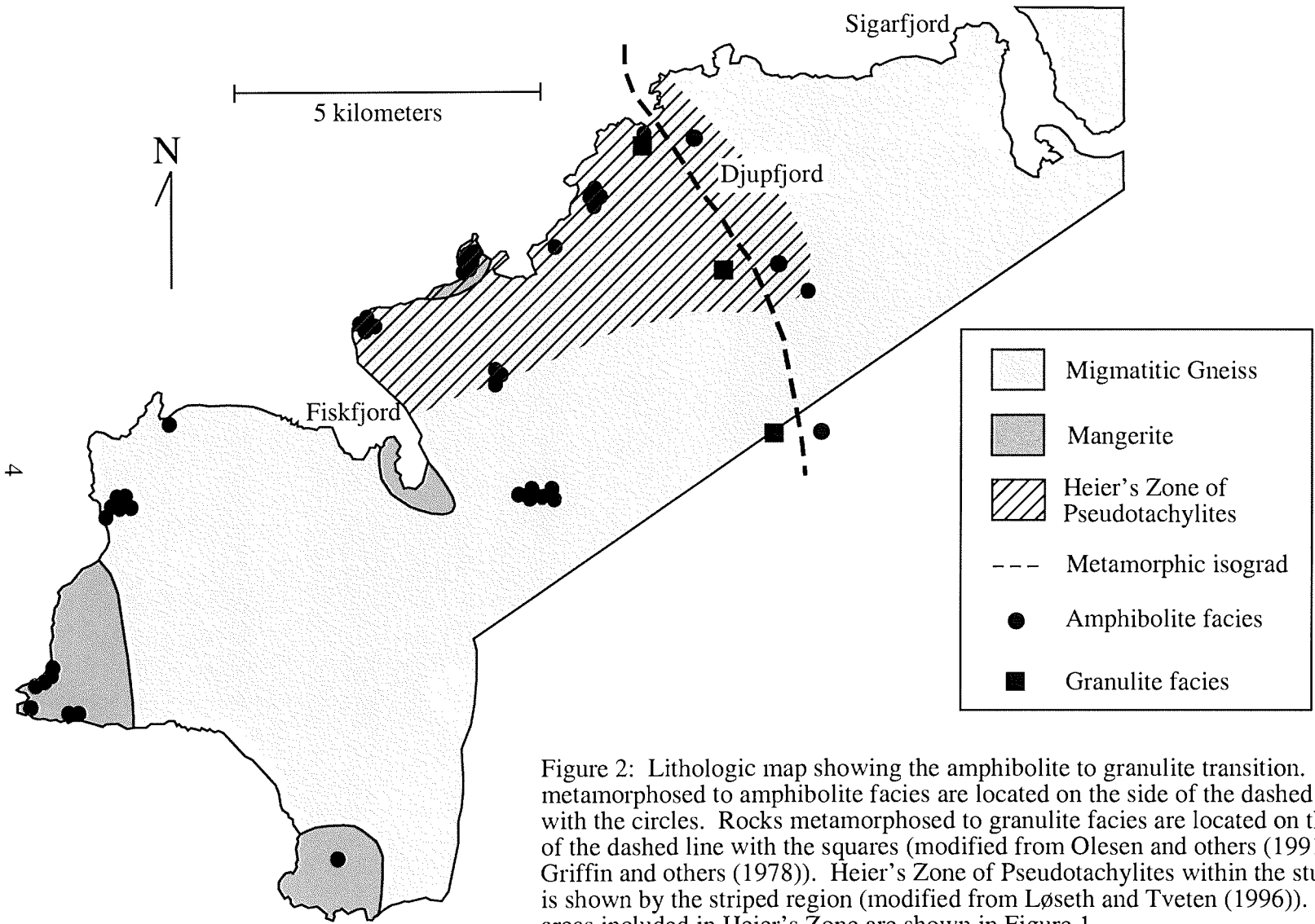

Figure 2: Lithologic map showing the amphibolite to granulite transition. Rocks metamorphosed to amphibolite facies are located on the side of the dashed line with the circles. Rocks metamorphosed to granulite facies are located on the side of the dashed line with the squares (modified from Olesen and others (1991) and Griffin and others (1978)). Heier's Zone of Pseudotachylites within the study area is shown by the striped region (modified from Løseth and Tveten (1996)). Other areas included in Heier's Zone are shown in Figure 1.

GEOLOGIC CONTEXT

The Caledonian Orogeny occurred during the Silurian and into the Early Devonian Periods (Roberts and Gee, 1985). The orogen is characterized by a series of nappes thrust eastward on to the Baltoscandian platform. These nappes are grouped into four complexes known, from bottom to top, as the Lower, Middle, Upper, and Uppermost Allochthons. Tectonostratigraphically below these nappes is the Autochthon and Parautochthon, containing the Precambrian crystalline basement rocks (Roberts and Gee, 1985). The particular area chosen for this study is western Hinnøy (Figure 1), which is underlain by the Precambrian basement. The bulk of the rocks exposed here are early Proterozoic supracrustals migmatitized at approximately 2,700 Ma and later intruded by 1.8 Ga mangerite plutons (Griffin et al., 1978). Dating by Griffin and others (1978) has been interpreted to indicate that metamorphism within these rocks occurred ca. 1830-1700 Ma.

The two major lithologies in the study area are migmatitic gneiss and mangerite. The gneiss underlies most of the area and the mangerite is located mostly in the southwestern part (Figure 3). The gneiss has very distinct compositional banding that can be measured but is often contorted, folded or anastomosing over a scale of two meters or less. It is a very heterogeneous rock, with bands of plagioclase and quartz alternating with bands of hornblende, pyroxene, and biotite. Mangerite is a plutonic rock of the

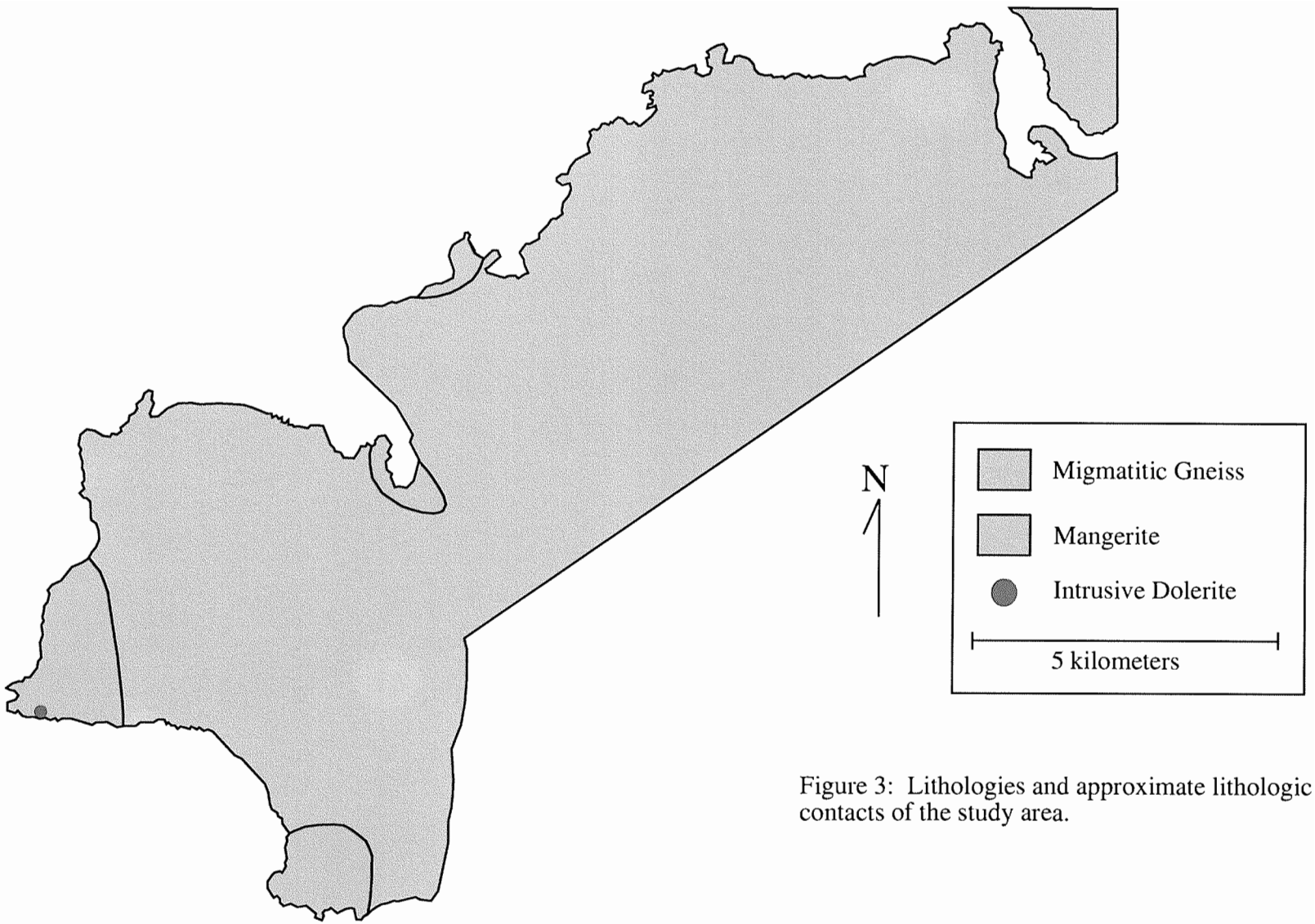

Figure 3: Lithologies and approximate lithologic contacts of the study area.

charnockite series corresponding to pyroxene monzonite (Bates and Jackson, 1987). It consists of plagioclase, pyroxene, and minor biotite. Grain size ranges from fine to very coarse in the space of a few meters. The contact between the migmatite and the mangerite is intrusive, with the mangerite being the younger intrusive phase.

Heier (1960) reported an extensive zone of pseudotachylite in and around the study area. Pseudotachylites are a glass or mixture of commuted mineral grains that appear as tachylites and are often formed through frictional melting associated with high-strain rate brittle faults. Although Løseth and Tveten (1996) show the known extent of Heier's Zone, they do not characterize the faults that appear to be associated with the zone in terms of their geometry or kinematics and, therefore, do not completely show the relationship between the faults and Heier's Zone. Many of these faults shown in Løseth and Tveten's (1996) report appear only inferred from topography and not actual field evidence. Some of these faults are and some are not associated with pseudotachylites. The same authors also interpreted some faults based on seismic profiles. An objective of this study is to confirm and structurally analyze these faults.

Olesen and others (1997) summarized the post-Caledonian faults in northern Norway and characterized them mainly by their orientation and geophysical signatures. However, their report focuses on offshore structures using seismic data and well logs. Very little data are presented about exposed faults and no rigorous structural or kinematic analysis is given. Paleomagnetic ages are presented for several faults, specifically one in the study area. The paleomagnetic age for this fault was interpreted to be Ordovician (Olesen et al., 1997); however, the interpretations appear to be somewhat speculative.

Davidsen and others (2001) discovered Mesozoic fossils in displaced boulders on the shore of west Hinnøy. These authors also reported marine seismic data from directly offshore, supporting a young extensional basin, possibly Jurassic in age; a similar Jurassic age basin is exposed on Andøya (Dalland, 1975), located further north of the study area. The orientation and timing of this fault would place Heier's Zone of Pseudotachylites in the hanging wall. However, Davidsen and others' (2001) evidence is entirely inferential.

Work by Markl (1998) on the petrology of the Eidsfjord anorthosite, on the island of Langøy, directly west of Hinnøy (Figure 1), indicates a major, low-angle thrust beneath the anorthosite pluton and Heier's Zone of Pseudotachylite. Since Markl (1998) presents little kinematic data and no microstructural information, it is impossible to discern at what level this structure formed in the crust or whether it truly is a thrust or, rather, a low-angle normal fault as per Davidsen and others (2001). The lack of timing information and its spatial association with Heier's Zone of Pseudotachylites have led some to believe that this structure, and others associated with it, are post-Caledonian extensional structures. An $^{40}Ar/^{39}Ar$ date on the pseudotachylites associated with this fault by Plattner and others (2003) suggests that this deformation is late-Caledonian in age. This estimate is reasonable, considering that there is no evidence supporting a late- to post-Caledonian contractional event in north central Norway.

METHODS

This project required both field and laboratory work. Two and a half months of field work were accomplished during the summer of 2000. Field work included mapping with base topographic maps (1:50,000) and a Brunton compass, collecting samples of local lithologies and oriented samples from structural features, and taking measurements of these features. Laboratory work consisted mainly of the microscopic analysis of 50 commercially made thin sections to determine the lithologies through a petrographic identification of all minerals as well as shear sense and microstructural development of shear zone and fault rocks. Data collected in the field were used to compile a lithologic and structural map of the area and to produce stereographic projections of the structural features for geometric and kinematic analysis. Seven samples were submitted for $^{40}Ar/^{39}Ar$ isotopic analysis in Mick Kunk's lab, USGS, Denver, Colorado. Software used in the preparation of this project included Canvas 7® for all graphics and figures, and Microsoft Office 98® for the text and presentation. All microscope and computer work was accomplished using facilities in the Department of Geology and Geography, Auburn University.

LITHOLOGY

There are two major lithologies found in this particular area of northwestern Hinnøy, migmatitic gneiss and mangerite. Along with these two major lithologies, there occurs an intrusive dolerite and many pseudotachylites. These rocks and the contacts between them are described below.

Migmatitic Gneiss

The migmatitic gneiss is the most voluminous rock in the area. It is typically a white and medium gray rock although some varieties contain copious amounts of potassium feldspar giving the rock a pink color (Figure 4a). Grain size varies from medium-coarse (3 – 5 mm) to coarse (up to 1 cm). At most localities this rock is coarsely banded, with the texture ranging from a chaotic to weakly foliated stromatolitic migmatite (Mehnert, 1968). Migmatite is comprised of white plagioclase and blue-gray quartz in the lighter colored bands and hornblende and minor biotite in the darker colored bands. The compositional banding ranges in thickness from one-to-two millimeters up to ten centimeters (Figure 4b). Minor muscovite and opaque minerals also occur. At some localities the feldspar is bright pink potassium feldspar, the quartz is blue and mafic minerals may be less abundant.

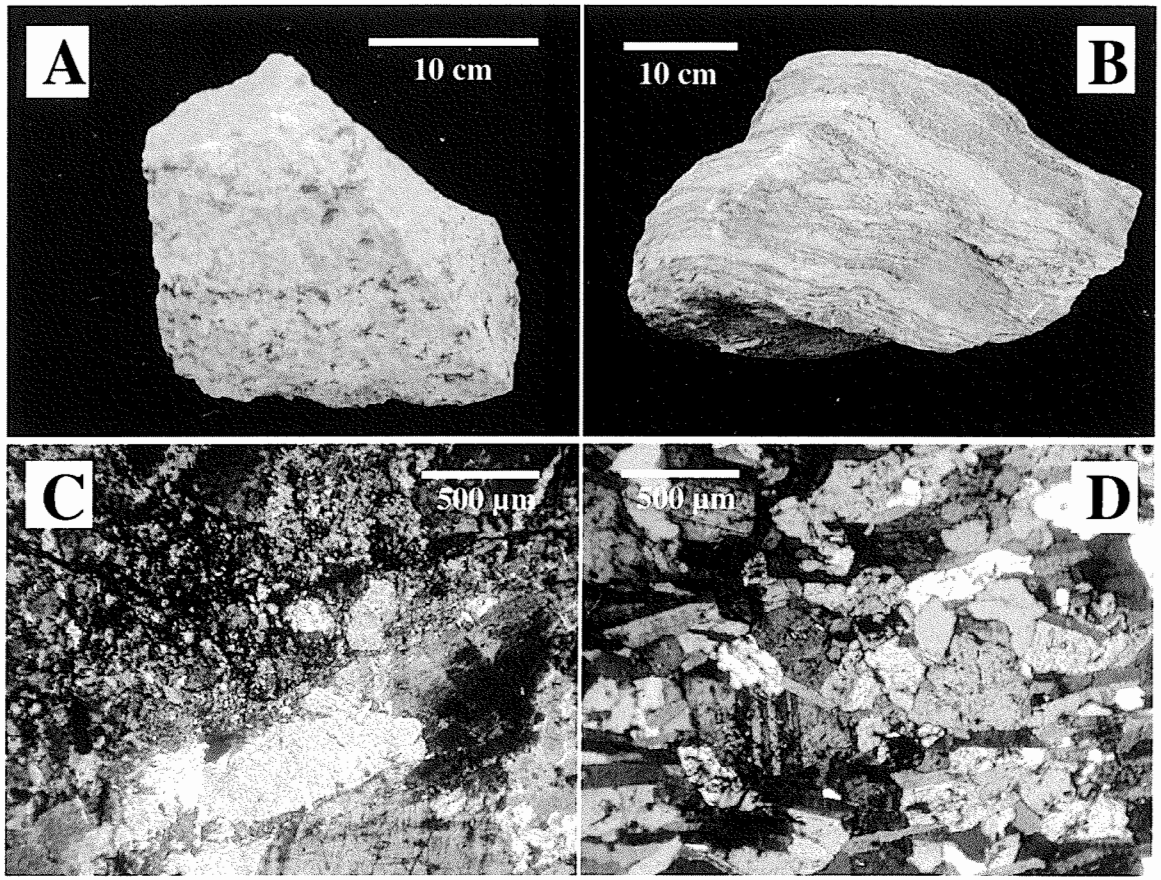

Figure 4: Samples of migmatitic gneiss showing variations within the lithology. A) Photograph of migmatitic gneiss with significant amounts of potassium feldspar. B) Photograph of migmatitic gneiss with more abundant mafic minerals. C) Thin section of migmatitic gneiss similar to the sample in (A) under crossed polars. D) Thin section of migmatitic gneiss similar to the sample in (B) under crossed polars.

In thin section quartz and plagioclase have undulose extinction and microcline is characterized by crosshatched twin lamellae. Quartz and plagioclase generally are equidimensional. Biotite and hornblende grains contain inclusions of plagioclase and quartz. Biotite may be chloritized along small fractures. Minerals in these rocks tend to be xenoblastic (Figure 4c and 4d). Several quartz-biotite schist and amphibolite xenoliths were observed in the migmatitic gneiss. The xenoliths were stretched parallel to the foliation. Minor flow folds and ductile shears are common. Transposition and destruction of the compositional banding locally is intense, generally in association with the folds and shears.

This lithology makes up the majority of the northeastern and central parts of the study area and probably correlates to the "Migmatitic gneiss" described by Hakkinen (1977) for areas directly north of Sigarfjord (Figure 1). Also, some varieties of finer-grained gneiss resemble Hakkinen's (1977) "Veined and Layered gneiss" to the north but the author was not able to separate these rocks into a mapable unit in the study area (Figure 3).

Mangerite

Mangerite crops out in the southwestern most part of the study area (Figure 3). The mangerite is separated from the migmatitic gneiss by an irregular contact that appears to be intrusive. In this study area, mangerite occurs as a massive medium to dark gray rock. It ranges from medium (1 – 2 mm) to very coarse-grained (> 1 cm) and commonly has a stained and pitted surface due to weathering. The mangerite contains coarse-grained mesoperthite, plagioclase, fine-grained biotite, clinopyroxene,

hypersthene, and fine-grained opaques. The mesoperthite has mottled extinction and a poikilitic texture (Figure 5).

Heier (1960) described similar 'porphyroblastic monzonitic granulites' on western Langøy that grade into more felsic, charnockitic gneisses. Similar mangerites and charnockites underlie the bulk of the Lofoten islands and parts of western Hinnøy (Tull, 1977; Griffin et al., 1978). Directly north and east of the study area, passing roughly through Sigarfjord, lies and orthopyroxene isograd separating granulite-facies rocks to the west from amphibolite-facies rocks to the east (Figure 2) (Heier, 1960; Griffin and Heier, 1969; Griffin et al., 1978, Olesen et al., 1991). Heier (1960) suggested that the granulites were retrograded to amphibolites and, hence, the term 'retrograded mangerite' has been used for rocks where, generally, pyroxene is replaced by amphibole. No amphibole was observed in the mangerite of the study area.

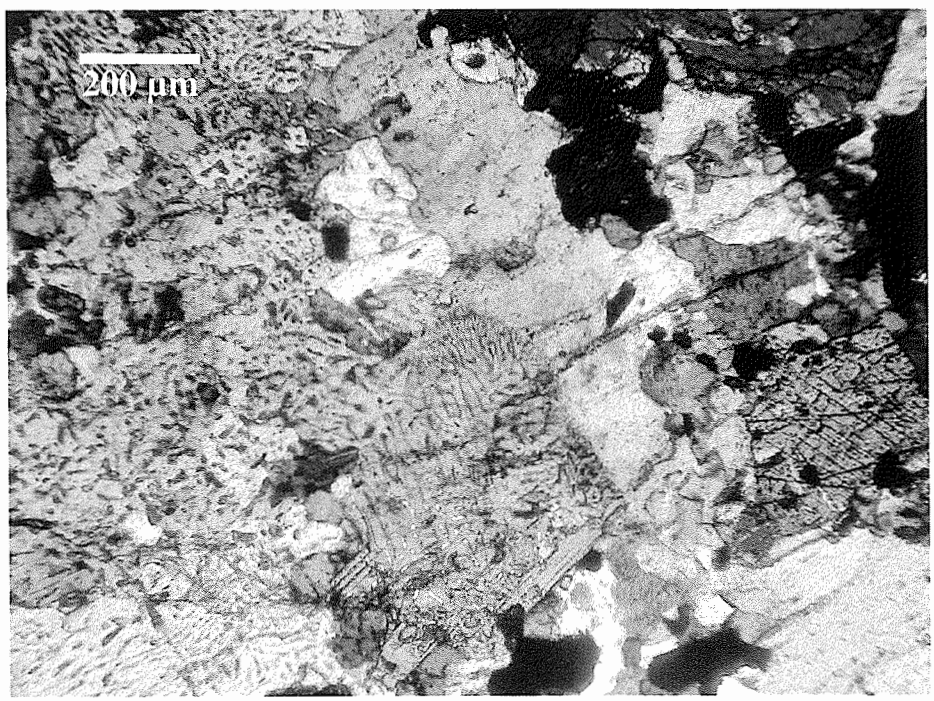

Figure 5: Thin section of mangerite sample from the study area under crossed polars showing mesoperthite textures.

Intrusive Dolerite

A small outcrop of dolerite was found in the area of mangerite (Figure 3). It is fine-grained (< 1mm), black, and contained laths of plagioclase set in a subophitic texture (Figure 6). The age and intrusive relations of the dolerite are not known. Direct contact with the mangerite was not visible. Misra and Griffin (1972) reported a swarm of vertical dolerite dikes in western Hinnøy and Austvågøy to which this injection might belong. Based on contact relations and corona textures of the dolerites it was suggested by Misra and Griffin (1972) that they intruded at intermediate crustal levels while the mangerites were still hot. Reports attempting to date the dolerite were unsuccessful (see Griffin et al., 1978) but the present author collected a sample that was analyzed for $^{40}Ar/^{39}Ar$ isotopic dating (see $^{40}Ar/^{39}Ar$ Isotopic Analysis section).

Figure 6: Thin section of the dolerite sample from the study area under crossed polars illustrating subophitic texture.

Pseudotachylites

Pseudotachylites occur in this area in both the gneiss and the mangerite, although they are much more common in the gneiss. They are found as dense, dark gray to black, microcrystalline rocks that occur in branching veins. Where they occur in large groups there is commonly a slightly larger main pseudotachylite vein from which many smaller veins branch off (Figure 7). Inclusions of the host rock can be found within these veins. They are commonly found along with faults, shear zones or brittle fractures, but locally they occur separate from these structures. They range from a few millimeters up to five or six centimeters in width (Figure 7) and are sometimes traceable for up to several meters in length. They occur mainly in two parts of the study area, along the west central margin and in the southwest (Figure 8). Those along the west central margin coincide with the documented location of Heier's Zone of Pseudotachylites (Løseth and Tveten, 1996), but those in the southwest do not (Figure 8). Where they are associated with a shear zone, they tend to occur in anastomosing groups. In thin section they appear as veins of extremely fine-grained crystals, too small to resolve with an optical microscope.

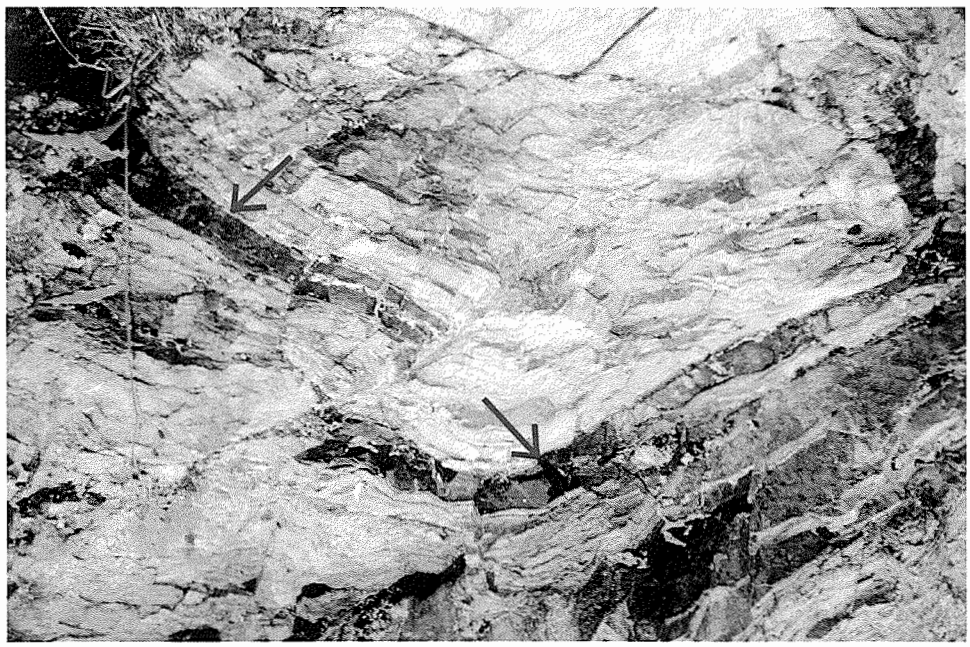

Figure 7a: Faulted pseudotachylite vein (arrows) found at an outcrop of migmatitic gneiss near Husvik in the study area. Approximate thickness of the vein is 5 cm.

Figure 7b: Pseudotachylite found coating the plane of the fault at Fiskfjord. View of pseudotachylite is perpendicular to strike and dip. Finger points along the direction of the slip line. Gray lines in the pseudotachylite are brittle fractures.

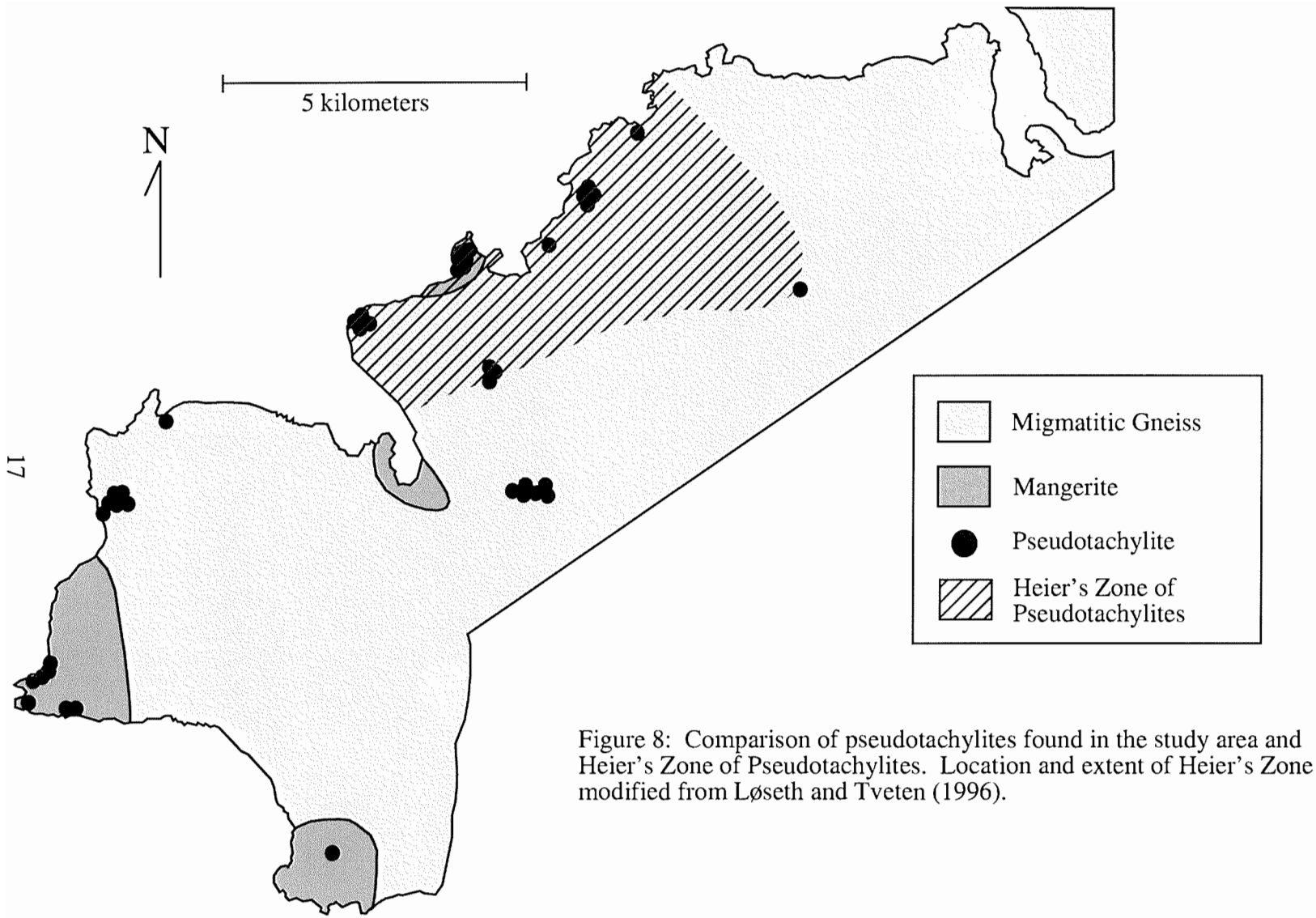

Figure 8: Comparison of pseudotachylites found in the study area and Heier's Zone of Pseudotachylites. Location and extent of Heier's Zone modified from Løseth and Tveten (1996).

METAMORPHISM

Rocks in this study area are reported to have been metamorphosed to granulite facies in the southern part, and to amphibolite facies in the northern part (Griffin, et al., 1978; Olesen et al., 1991)(Figure 2). Olesen and others (1991) suggest that this transition effectively marks a surficial exposure of an ancient Conrad discontinuity. The Conrad discontinuity is a seismic velocity discontinuity within the Earth's crust that is equivalent to the boundary between the upper crust and lower crust below which velocities increase (Bates and Jackson, 1987). Thus, Lofoten-Vesterålen may preserve a considerably thick section through the ancient continental lithosphere underlying western Baltica. Isotopic dating by Griffin and others (1978) has been interpreted to indicate that this Conrad discontinuity formed at ca. 1830 – 1700 Ma.

It is generally agreed that Caledonian metamorphism of the Precambrian basement in Lofoten-Vesterålen was limited by the availability of fluids to drive metamorphic reactions (Griffin et al., 1978; Bartley, 1982). The only rocks in this area that appear to show effects of Caledonian metamorphism/deformation are those affected by crystal-plastic and brittle shearing. $^{40}Ar/^{39}Ar$ isotopic investigations launched by the present study (see below) were intended to provide insights into the distribution of the Caledonian effects in this area.

The predominantly granitoidal composition of rocks in the study area does not easily allow determination of metamorphic conditions using petrogenetic grids. Nonetheless, the migmatitic gneiss does show a variation in its metamorphic assemblage over the study area that is not considered a function of bulk composition, but rather a function of metamorphic grade. In the northern part where Griffin and others (1978) indicate that rocks were metamorphosed to amphibolite-facies conditions, the migmatitic gneiss has the assemblage: quartz + oligoclase + biotite + hornblende + muscovite, similar to the lithology in Figure 4d. In the southern part where Griffin and others (1978) indicate that rocks were metamorphosed to granulite-facies conditions, the felsic gneiss contains the assemblage: quartz + potassium feldspar + biotite + hornblende + plagioclase, similar to the lithology in Figure 4c. The growth of potassium feldspar at the expense of muscovite indicates the crossing of the muscovite-out reaction at relatively high temperatures (Spear, 1993).

The mangerite, which occurs in the southernmost part of the study area and in spotty occurrences along the shoreline, clearly documents granulite-facies conditions of metamorphism. The mangerite has the assemblage: mesoperthite + plagioclase + orthopyroxene + clinopyroxene + biotite (Figure 5).

A few exposures of rocks of basaltic composition help to further constrain metamorphic conditions. Mafic xenoliths and 20 centimeter-thick interlayers of amphibolite occur within gneisses in the northern part of the field area near Husvik. The amphibolites contain the assemblage: hornblende + biotite ± plagioclase ± garnet, which commonly is reported in amphibolite-facies terranes (Spear, 1993).

The dolerite intrusion, which occurs in the southern part of the study area (Figure 3), contains neither amphibolite- nor granulite-facies assemblages. Rather it has the assemblage: plagioclase + biotite + pyroxene + opaque minerals (Figure 6). This may indicate that the dolerite postdated the Precambrian metamorphic event. If it is a pre-Caledonian intrusion it is very likely that it escaped any alteration at that time, probably due to the aforementioned limited availability of fluids.

Proterozoic retrograde metamorphism in the northern part of the study area is shown by the gradual change from granulite- to amphibolite-facies assemblages toward the north (Griffin et al., 1978). A gradation such as this may be due to a greater availability of fluids in rocks toward the north (Bartley, 1982). Evidence for alteration subsequent to the 1.8 Ga event is shown by the occurrence of epidote along fractures in a few outcrops of migmatitic gneiss (Figure 9).

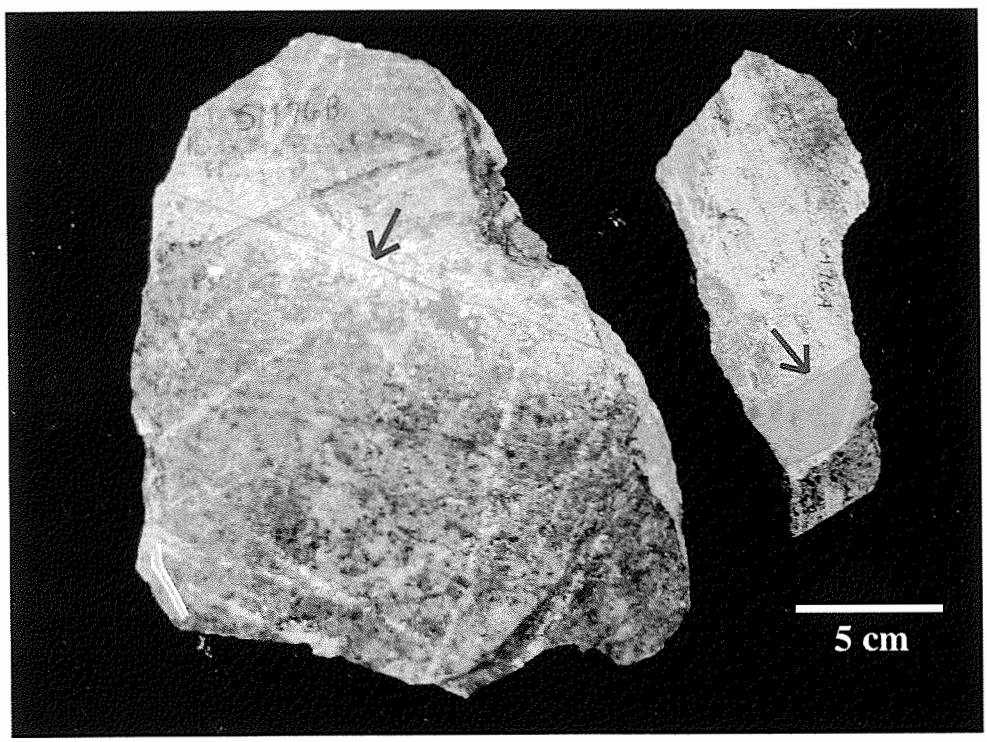

Figure 9: Alteration and epidotization by hot fluids along fractures (arrows). Rock is a mangerite with multiple fracture sets.

Evidence of retrogression is the occurrence of chlorite that has partially replaced biotite (Figure 10). Retrogression to chlorite is most commonly found in the migmatitic gneiss of the northern part of the study area. The rocks in this area show the retrograded assemblage: quartz + sausseritized plagioclase + chlorite. Chloritized biotite is also found in a few mylonites from shear zones where it may be related to Caledonian shearing and not Precambrian metamorphism.

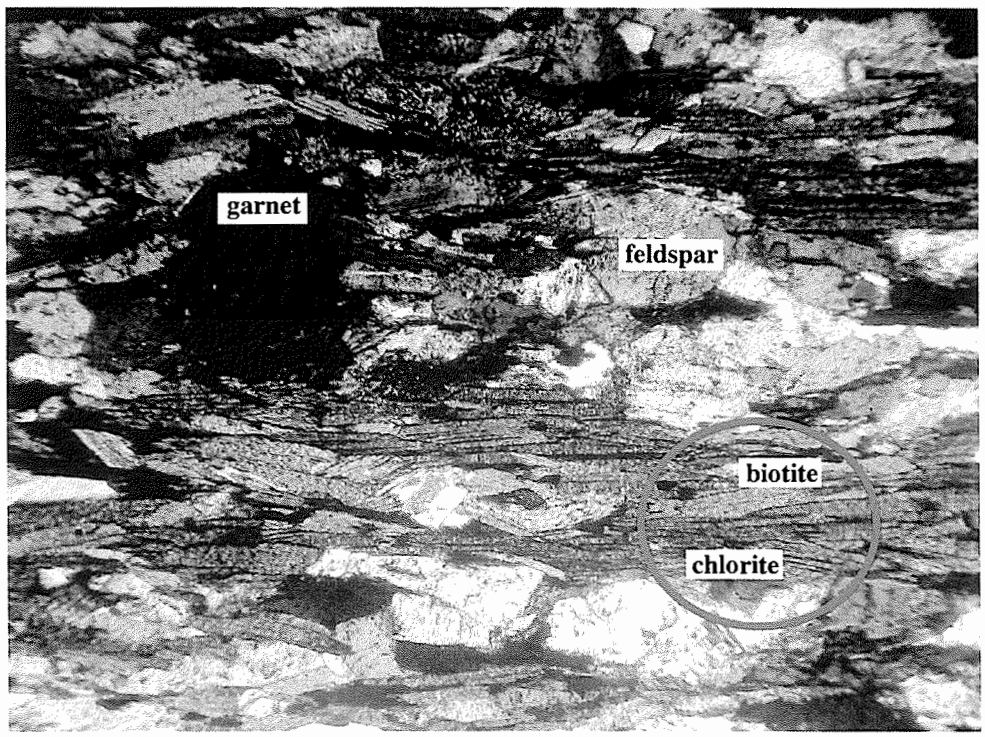

Figure 10: Thin section showing chloritization of biotite (inside circle) within a ductile shear zone (see structure section).

STRUCTURE

Precambrian, Caledonian, and post-Caledonian structures are all likely to be present in rocks of this study area. Analyses of these features were done mainly on a mesoscopic and/or microscopic scale for several reasons. The first reason is the discontinuous nature of the rocks, which is fairly typical of Precambrian continental basement complexes worldwide. The lack of marker units, the chaotic nature of the migmatitic gneiss, and the non-planar plutonic contacts made analysis of map-scale structures difficult. Second, outcrops in this area are generally spotty. Only along the shoreline and high on mountain ridges were rocks continuously exposed. Otherwise, grasses, bogs, and forests covered the bedrock. The intensity of the late-stage brittle fracturing and shearing also has complicated earlier features. Even the later features were only visible on a mesoscopic scale and could not be confidently traced over significant distances within the study area. The result is that the geologic map (Figure 11) mainly is an outcrop map, and contacts are inferred from outcrop to outcrop.

Compositional Layering, Gneissosity, and Schistosity

The compositional layering in rocks of the study is most likely a result of differentiation and migmatization during formation of the gneiss. Gneissosity is defined by light-colored bands of feldspar and quartz alternating with dark bands of hornblende

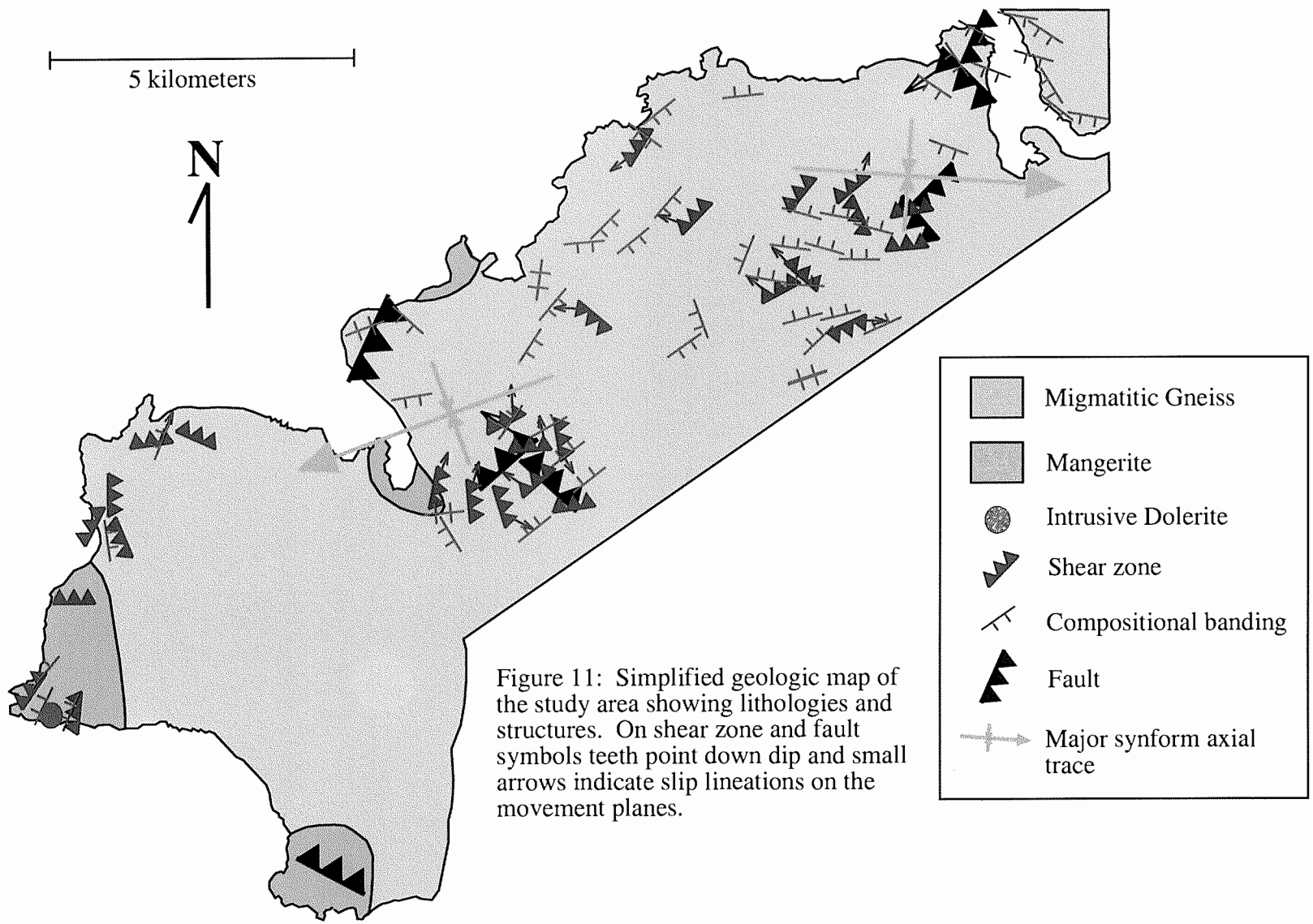

Figure 11: Simplified geologic map of the study area showing lithologies and structures. On shear zone and fault symbols teeth point down dip and small arrows indicate slip lineations on the movement planes.

and/or pyroxene, garnet, and biotite. These bands occur on the scale of a couple of millimeters to up to ten centimeters. In gneisses with a low percentage of mafic minerals, schistosity is more evident. Aligned biotite or muscovite grains define the foliation in these rocks. In all occurrences, the gneissosity and schistosity define and/or parallel the compositional layering.

Referring to Figure 12a, the stereogram for poles to compositional banding from the entire study area shows a great circle pattern striking 342, dipping 38° NE. Generally, compositional layering dips shallowly toward the west. This great circle distribution is interpreted to show that compositional layering orientation in this area can be used to find large-scale folds as discussed below.

In Figure 13, the study area is broken down into subareas. In the northern part, subarea A shows a point maximum of poles to compositional layering at 014 44°, and subarea B shows a point maximum at 187 24°. Subarea C has three point maxima at 047 37°, 349 18°, and 315 31°. Subarea D shows a partial great circle trend striking 340 and dipping 25° NE. Subareas E and F have point maxima at 142 30° and 111 32° respectively. The variations in orientation of compositional layering between the subareas may be a result of later deformation, as discussed below.

Folds

Two main styles of folds, termed early- and late-phase with respect to development of the principal metamorphic fabric, were observed in the study area. Early-phase, syn-metamorphic folds are tight to isoclinal in form (Figure 14a). The axial surfaces of the early folds invariably parallel the schistosity and gneissosity of the rock,

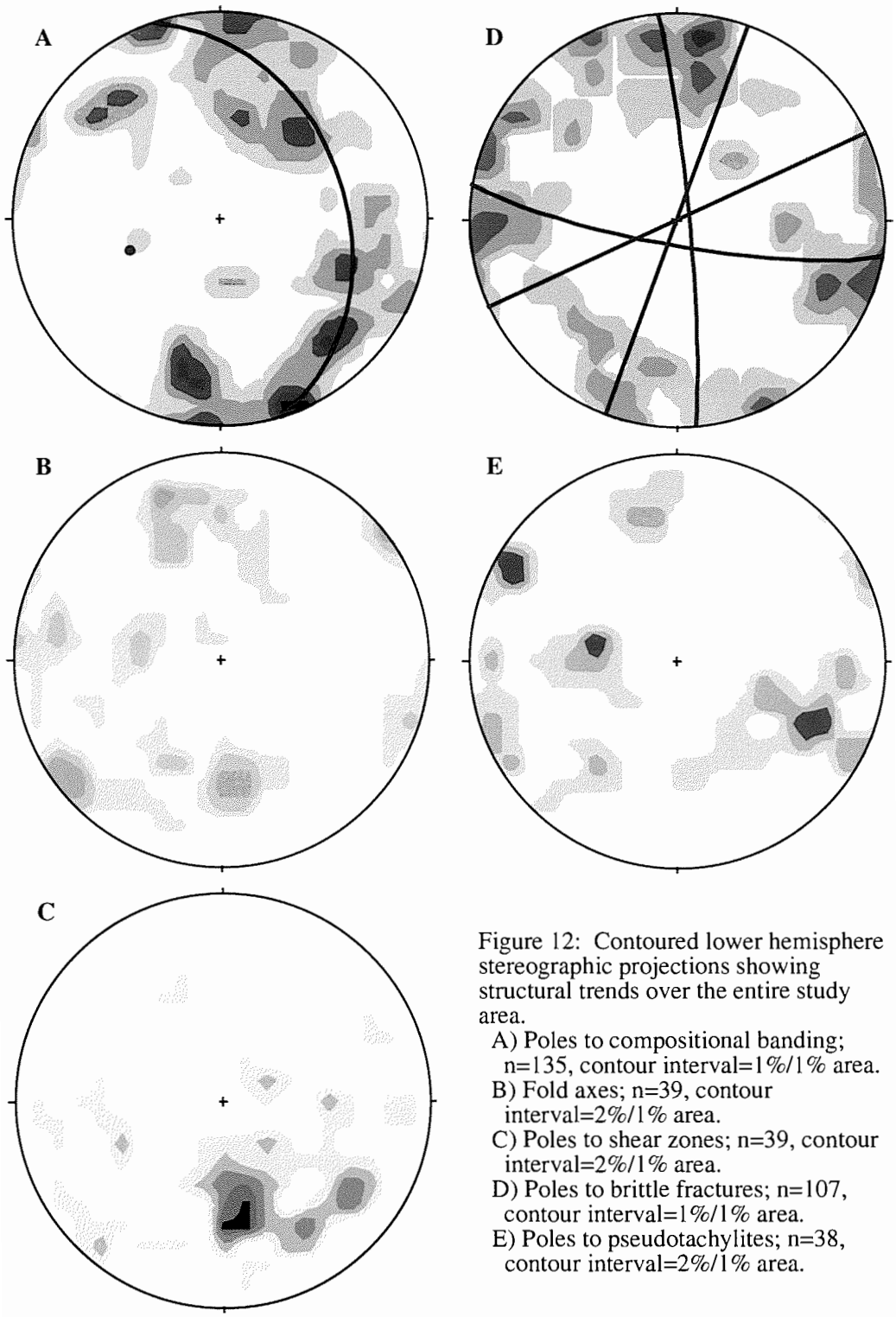

Figure 12: Contoured lower hemisphere stereographic projections showing structural trends over the entire study area.
A) Poles to compositional banding; n=135, contour interval=1%/1% area.
B) Fold axes; n=39, contour interval=2%/1% area.
C) Poles to shear zones; n=39, contour interval=2%/1% area.
D) Poles to brittle fractures; n=107, contour interval=1%/1% area.
E) Poles to pseudotachylites; n=38, contour interval=2%/1% area.

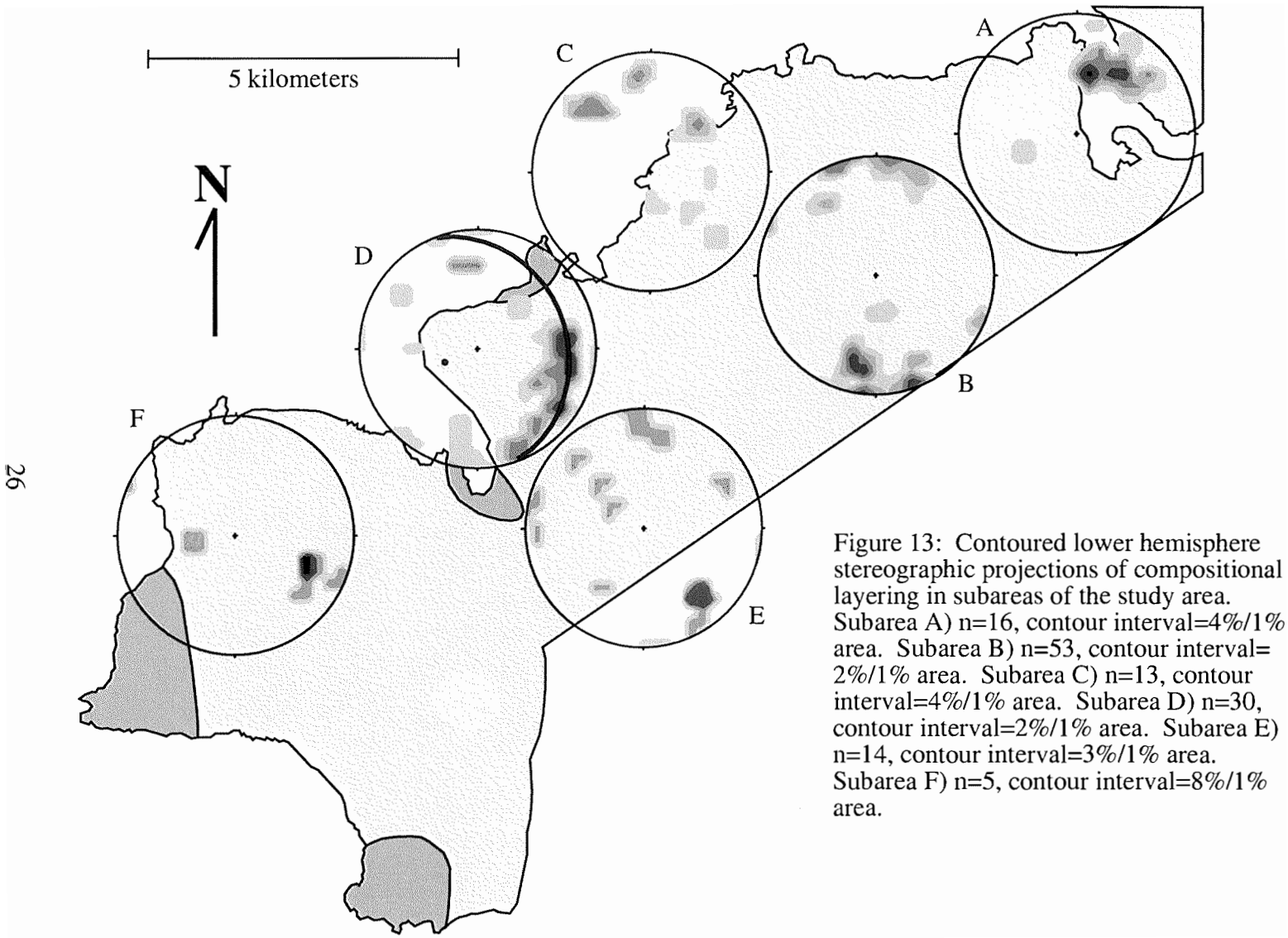

Figure 13: Contoured lower hemisphere stereographic projections of compositional layering in subareas of the study area. Subarea A) n=16, contour interval=4%/1% area. Subarea B) n=53, contour interval= 2%/1% area. Subarea C) n=13, contour interval=4%/1% area. Subarea D) n=30, contour interval=2%/1% area. Subarea E) n=14, contour interval=3%/1% area. Subarea F) n=5, contour interval=8%/1% area.

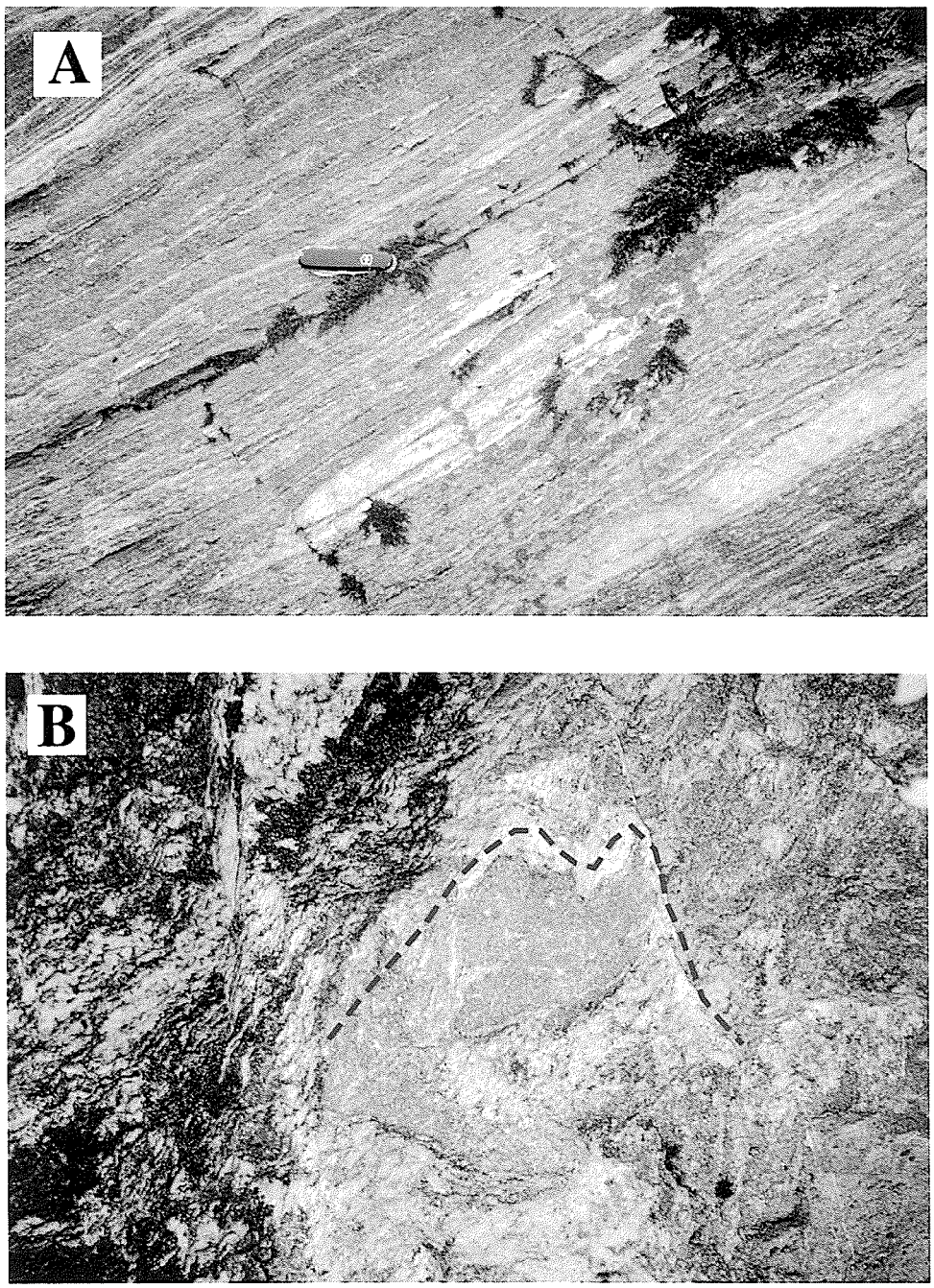

Figure 14: A) An early synmetamorphic isocline in a felsic layer within migmatitic gneiss in lower center of photo. Outcrop located near Sigarfjord. B) Late-phase post-metamorphic fold in migmatitic gneiss. Dashed red line outlines folded layer. Outcrop located near Sigarfjord.

whereas the compositional layering is wrapped around the fold nose. Thin sections document that metamorphic phyllosilicates and flattened tectosilicates pass undeflected through the fold nose, parallel with the limbs, and define the planar metamorphic fabric. Late-phase folds clearly deform the metamorphic foliation and compositional layering and, thus, are post-metamorphic folds (Figure 14b). The geometry of these folds is more open with more rounded hinges. The late-phase folds control the geometry of major folds depicted in Figure 11 and are indicated in stereoplots containing great circle distributions (i.e. Figures 12a and 13d). The folds that were observed on the outcrop scale may or may not be characteristic of map-scale folds throughout the area.

The axes for all these folds are shown in contoured lower hemisphere stereograms for the entire study area (Figure 12b) and for subareas (Figure 15); however, very few trends are evident. Early-phase folds are more common than late-stage folds, especially within the northeastern part of the study area. Late-phase folds are more common in the south, particularly within the mangerite. Most of these folds are visible at a small scale. Dimensions of these folds range from less than ten centimeters to no more than five meters. They are only traceable within the outcrop at which they occur. Larger-scale folds in this area are difficult to define given the fact that the rocks had been previously metamorphosed and deformed in the Precambrian and because contacts between units mainly are intrusive and irregular and are not tabular. The fold axis stereogram for the entire study area (Figure 12b) shows three general trends, 232 10°, 175 30°, and 339 14°. The first of these is roughly similar to the pole of the great circle distribution of poles to the compositional layering as seen in Figure 12a. It stands to reason, then, that the

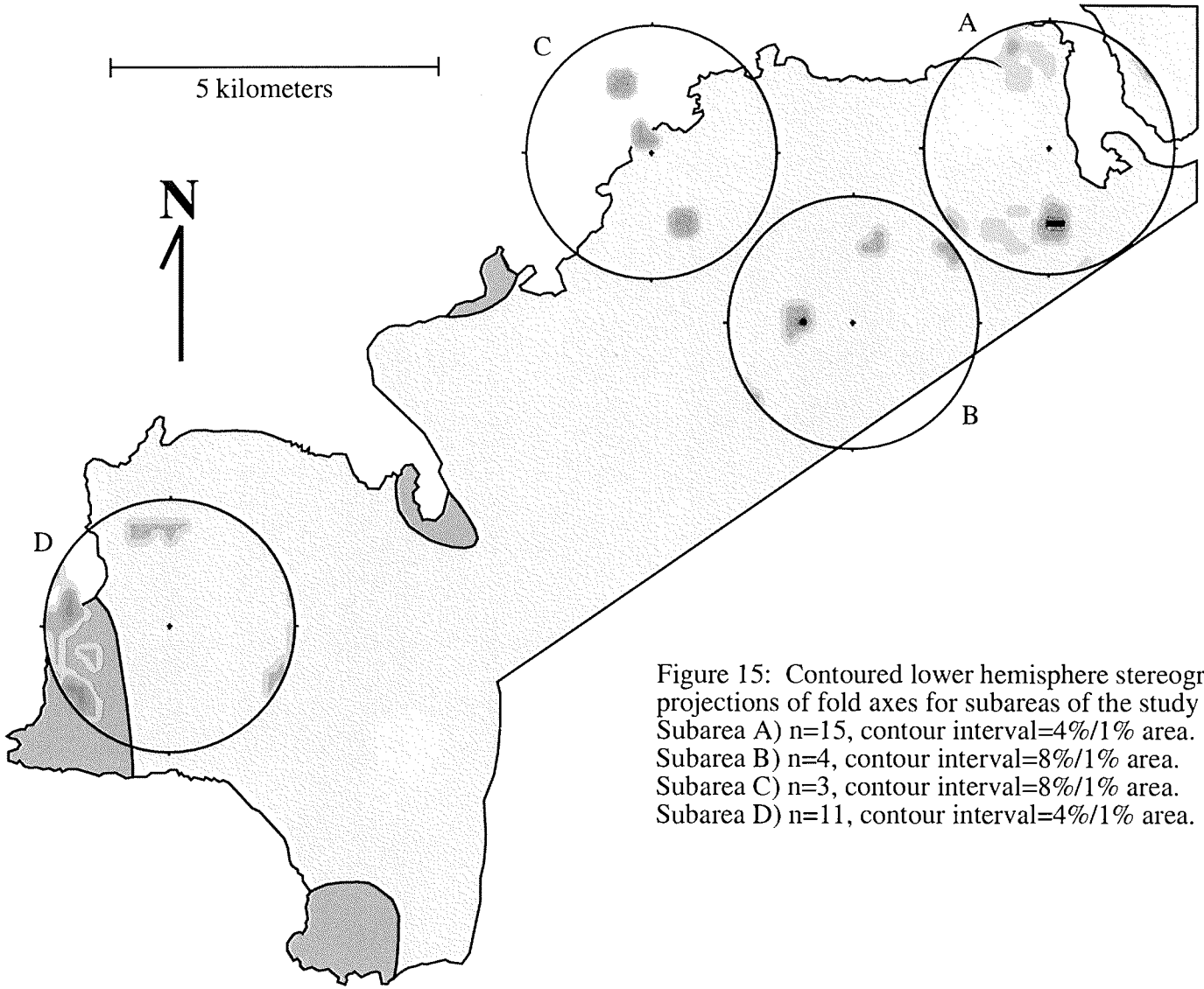

Figure 15: Contoured lower hemisphere stereographic projections of fold axes for subareas of the study area.
Subarea A) n=15, contour interval=4%/1% area.
Subarea B) n=4, contour interval=8%/1% area.
Subarea C) n=3, contour interval=8%/1% area.
Subarea D) n=11, contour interval=4%/1% area.

overall distribution of compositional layering trends resulted from the late-phase folding of rocks across the study area about an axis oriented roughly 232 10°.

In the northeastern part of Figure 13, subareas A and B each have distinctive point maxima of compositional layering at 010 45° and 195 22°, respectively. These appear to define limbs of a synform with a fold axis trending 094 and plunging slightly to the east (Figure 16). Subareas C, D, E, and F display pole distributions indicating the trend of another fold (Figure 16). This fold is interpreted as a synform with an axis trending close to the pole of the great circle in subarea D, 250 65°. Two of the point maxima in subarea C indicate the northern limb, whereas subareas E and F define the southern limb.

Shear Zones

Shear zones in this study are defined by cataclasites, mylonites, and ultramylonites and demonstrate semi-brittle to plastic behavior of these quartz-feldspar dominated rocks (Figure 17). The shear zones are rather narrow, ranging in thickness from 4 centimeters to up to one meter in the most highly deformed central part and no more than a meter thick in the less deformed protomylonitic shoulders (Figure 17b). Their extent parallel to strike is generally short; they are only traceable for a few meters and, thus, are difficult to depict at the scale of the map (Figure 18). Individual shear zones may be much more extensive but outcrop density and size often did not allow proof of it. Shear sense was mostly indeterminate at the outcrop scale; at only one or two locations were there shear sense indicators large enough to see and determine shear sense. Most shear sense indicators were visible only in oriented thin sections and are described below.

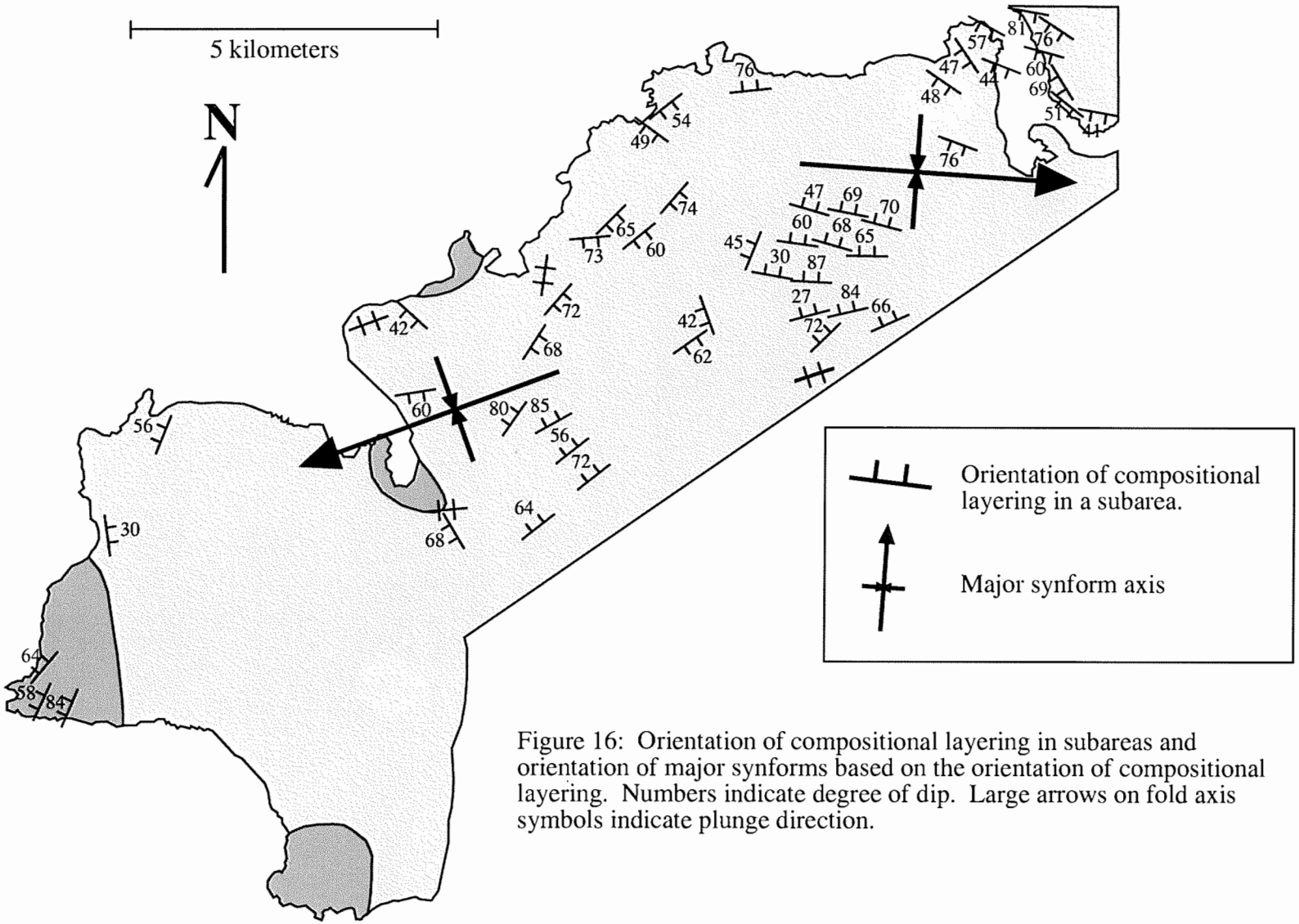

Figure 16: Orientation of compositional layering in subareas and orientation of major synforms based on the orientation of compositional layering. Numbers indicate degree of dip. Large arrows on fold axis symbols indicate plunge direction.

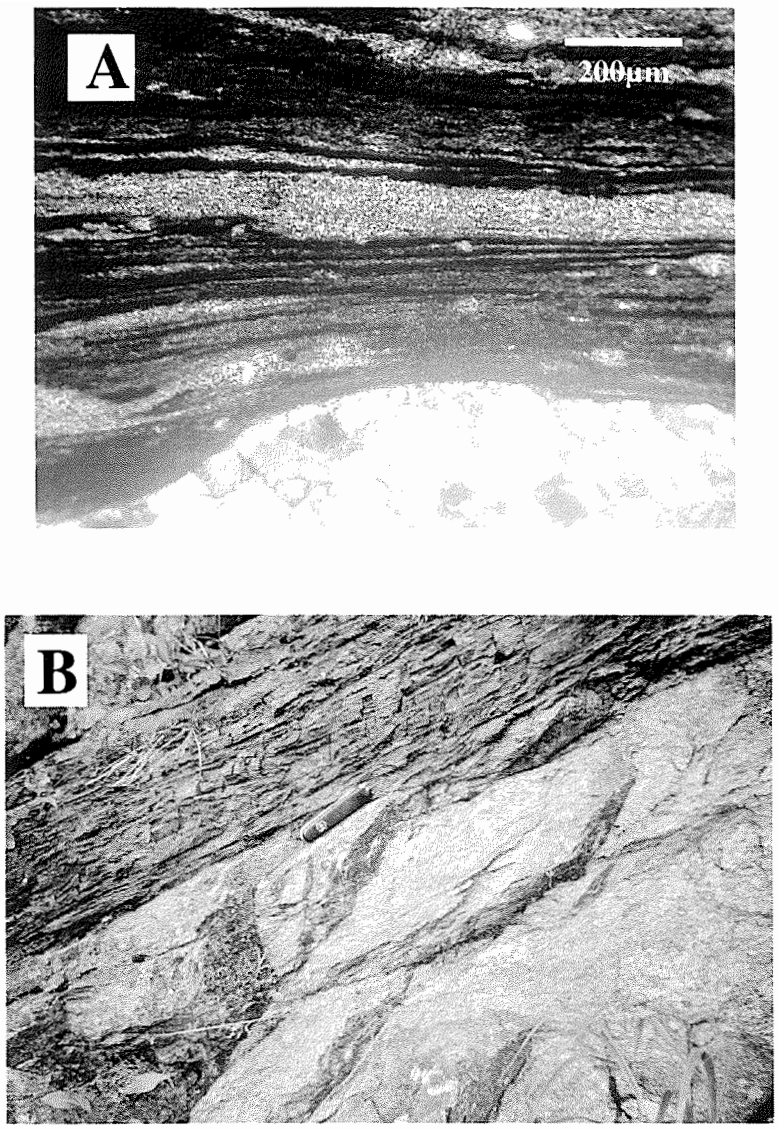

Figure 17: A) Thin section photograph of microstructures in the shear zone at Fiskfjord (pictured in (B)). The bottom is a large composite quartz grain. Mylonitic layering parallels long dimension of photo. Shear sense is sinistral. Dark bands are mostly biotite paste and lighter bands are recrystallized feldspar. (B) Crystal-plastic shear zone found at Fiskfjord. Shear zone is approximately 25 cm thick (tilted center left to upper right) with undeformed migmatite shoulder rocks above and below.

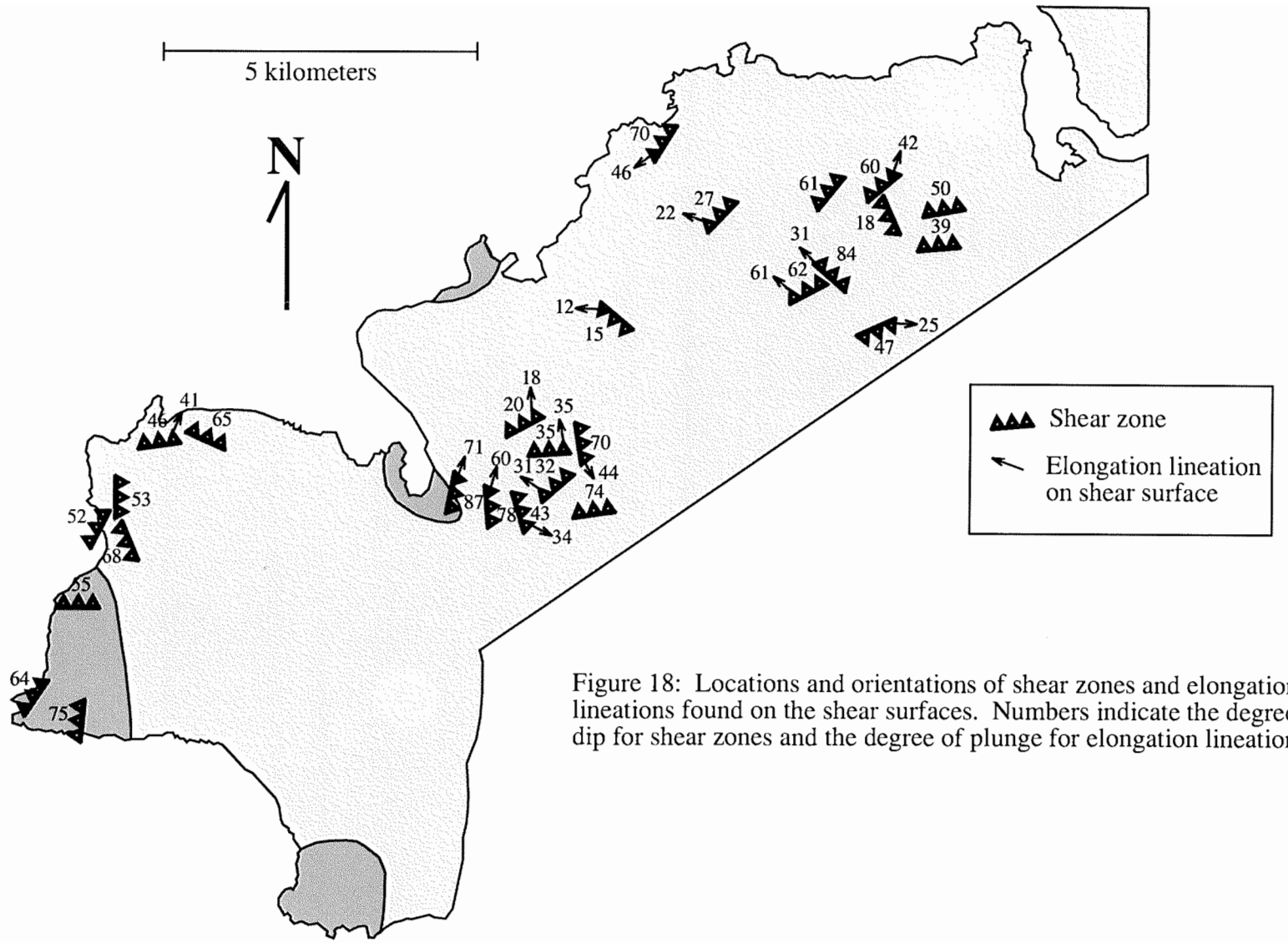

Figure 18: Locations and orientations of shear zones and elongation lineations found on the shear surfaces. Numbers indicate the degree of dip for shear zones and the degree of plunge for elongation lineations.

It appears that the shear zones occur in two sets over the study area (Figure 18). One set has a northeast strike and a northwest dip; the other has a northwest strike and either a northeast or a very shallow southwest dip. In four locations shear zones from both sets occur within ten meters of each other (Figure 19). In two of these four instances (locations 58 and 85, Figure 19) elongation lineations found on shear planes striking at roughly 90° to each other have subparallel slip lines (Figure 20a and 20b). Because of this it is inferred that both sets of shear zones were formed during the same event. Only in one of these four locations (location 125, Figure 20c) were shear zones from different sets observed to interact. At this location it was clear that the northeast-striking zone was formed first (Figure 21). However, in this case the northwest-striking zone was dipping to the southwest. At the one other location where two shear zones occur in close proximity (location 135, Figure 20d), there is no evidence that the direction of displacement on each was close to being subparallel. Here too, the northwest-striking shear zone dips toward the southwest. It is likely, then, that the northwest-striking, southwest-dipping shear zones formed at a later time than those that dip to the northeast did.

Hartman's treatment was applied to pairs of shear zones with one striking northeast and one northwest, where they were found together or in close proximity (Figure 20). In the two cases where the northwest-striking shear zone was dipping to the northeast the results of Hartman's treatment were very similar. In the two cases where the northwest-striking shear zone was dipping to the southwest, the results were quite different. The results from the first two cases show that movement along the northeast-

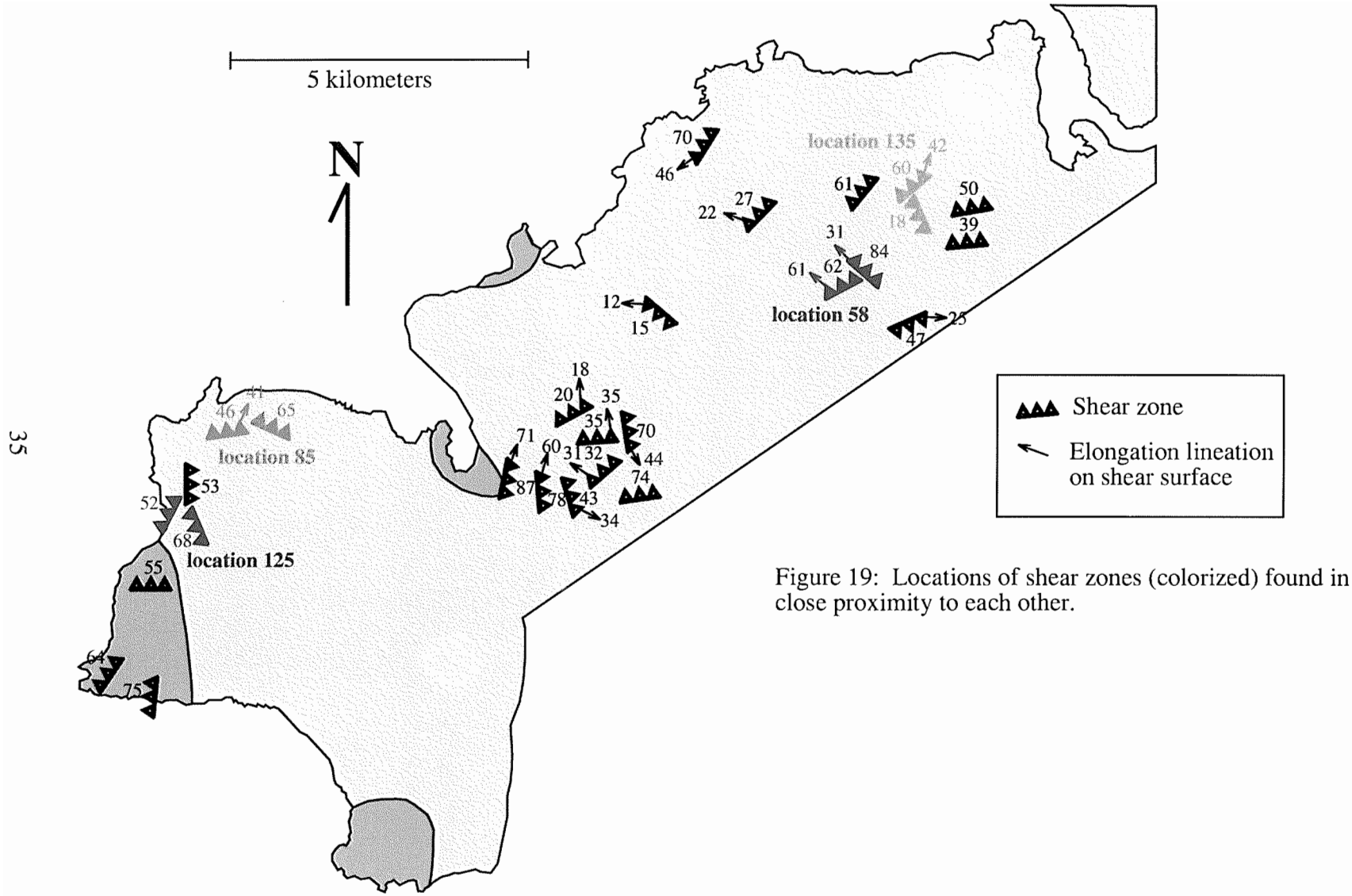

Figure 19: Locations of shear zones (colorized) found in close proximity to each other.

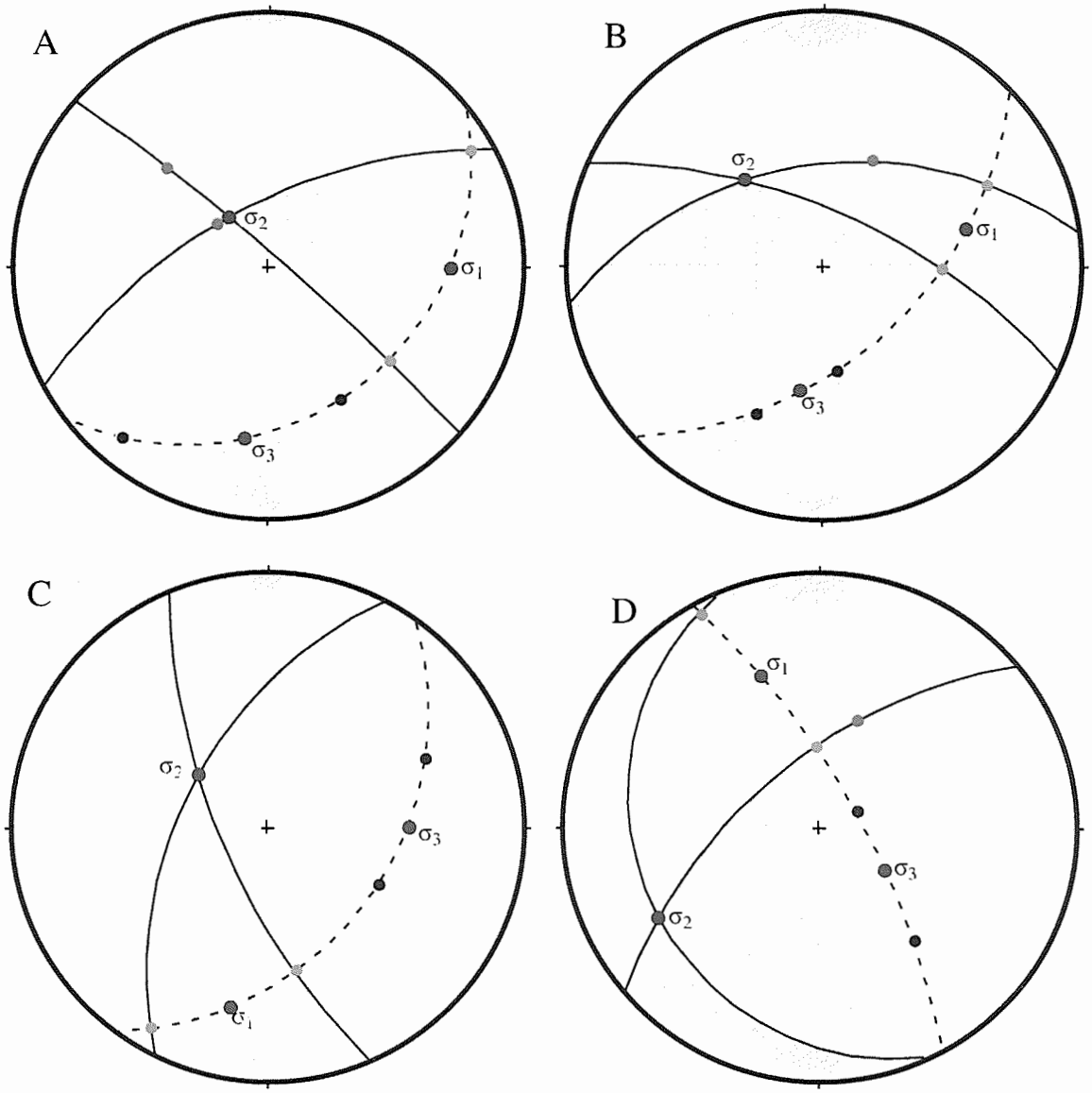

Figure 20: Hartman's treatment of paired shear zones as conjugate shears in equal angle, lower hemisphere stereoplots. (A) location 58, (B) location 85, (C) location 125, (D) location 135 (refer to figure 19 for locations). Black dots on the stereograms represent poles to the shear zones. Green dots are lineations found on the shear surfaces. Blue dots are theoretical lineations determined by Hartman's treatment. Red dots indicate the orientations of sigma 1 (acute bisectrix), sigma 2 (intersection of the planes), and sigma 3 (obtuse bisectrix). The dashed line is the sigma 2 principal plane.

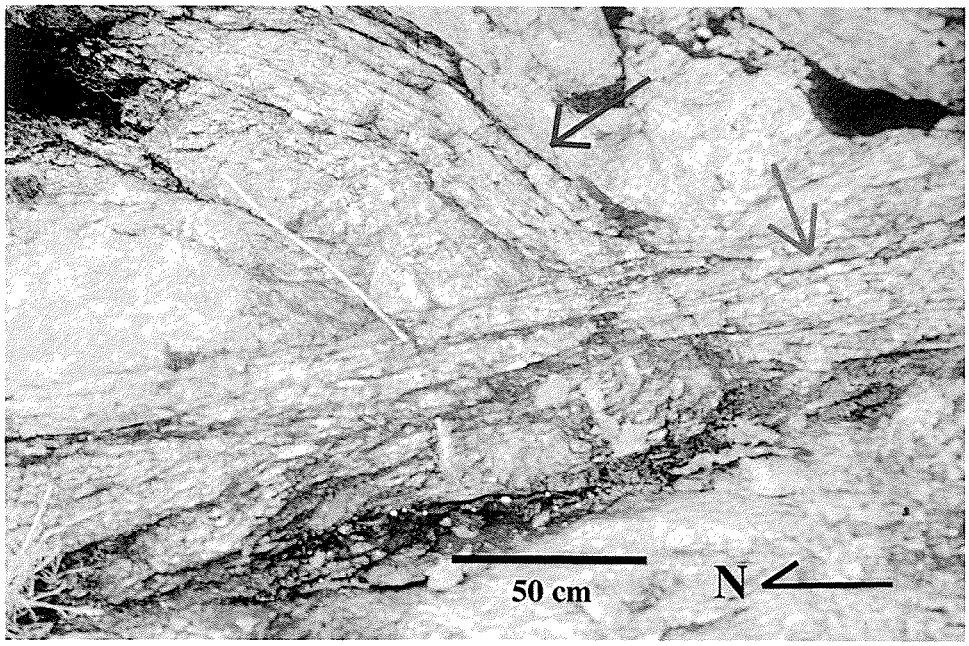

Figure 21: Interacting shear zones at location 125 (see figure 19). The northeast-striking shear zone, indicated by the red arrow, clearly is truncated by the northwest-striking shear zone, indicated by the green arrow. The approximate direction of north is indicated in the lower right corner of the photograph.

striking shear zones was oblique-dextral reverse and movement along the northwest-striking shear zones was oblique-sinistral normal (Figure 20).

The stereoplot of poles to all of the shear zones from the study area (Figure 12c) shows a point maximum at 174 38°, indicating a general shallow north-northwest dip. Dividing the area into subareas (Figure 22) shows a few consistent trends. Subarea A has a point maximum similar to the trend of the entire area. Subareas B, C, and E have a scattering of point maxima, and subarea D has a great circle trend at approximately 046 49° SE. Each of the subareas has shear zones striking to the northeast. Only subareas C and D also have shear zones striking to the northwest. As described, there are most likely

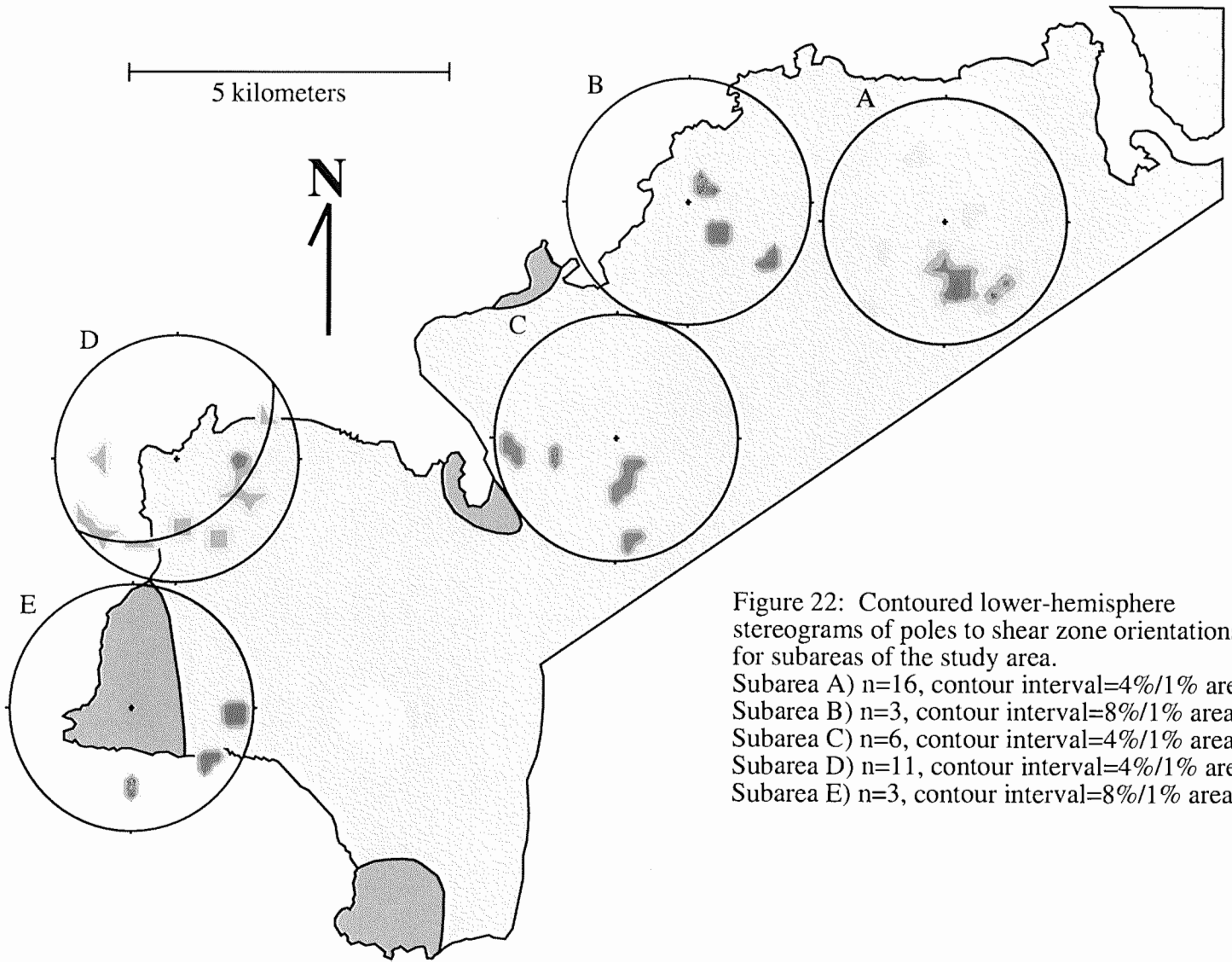

Figure 22: Contoured lower-hemisphere stereograms of poles to shear zone orientations for subareas of the study area.
Subarea A) n=16, contour interval=4%/1% area.
Subarea B) n=3, contour interval=8%/1% area.
Subarea C) n=6, contour interval=4%/1% area.
Subarea D) n=11, contour interval=4%/1% area.
Subarea E) n=3, contour interval=8%/1% area.

several sets of shear zones based on their geometry and kinematics. Generally, the steeper dipping ones (>60° dip) have elongation lineations that are shallow plunging. This indicates oblique, strike-slip motion (Figure 18). The shallower dipping shear zones have mostly down-dip elongation lineations that dip mainly to the west. This, along with kinematic indicators, indicates normal dip-slip motion.

In thin section, sigma and delta clasts of plagioclase feldspar, mica fish, and shear bands all provide shear sense indications (Figures 10 and 17a). Other microstructures include lattice preferred orientation, grain-shape preferred orientation in quartz, fractured and displaced feldspars with undulose extinction, ribbons of annealed quartz with triple-point grain boundaries, recrystallized feldspar and biotite, and fractured garnets with inclusions (Figures 10 and 17a). These features are indicative of crystal-plastic deformation of quartz, muscovite, and biotite, and brittle-plastic deformation of feldspar during shear zone formation. These microstructures indicate greenschist facies conditions between ~300 and 450° C (Scholz, 1988; Tullis, 1983).

Pseudotachylites (see below) are found associated with some of the shear zones. However, they are most commonly included within or proximal to the zone, implying that they were formed before or simultaneously with the shear zones. In no cases were pseudotachylites found to cut across shear zones.

Brittle Faults

Eight meso/macroscopic brittle faults were observed in the area (Figures 23 and 24). All of those observed have a major plane along which brittle deformation and displacement has occurred. They are interpreted to reflect both contractional and

Figure 23a: Photograph of the large shallow-dipping fault at Husvik (figure 24). Arrow points to fault plane. View is about 10 meters wide and faces to the south.

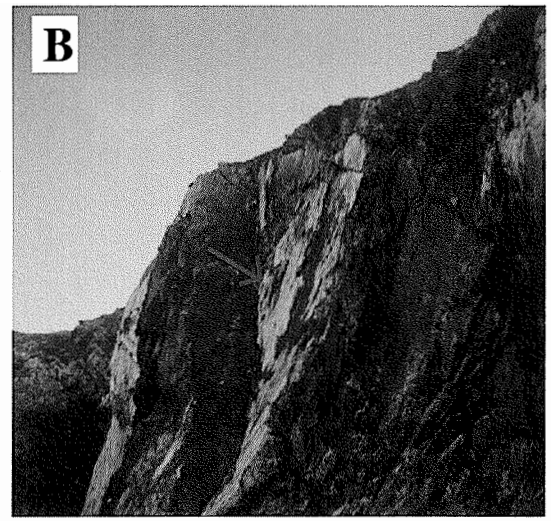

Figure 23b: Photograph of the quarry fault (figure 24). Arrow points to fault surface. Cliff face is approximately 75 meters high. View of photo is to the southeast.

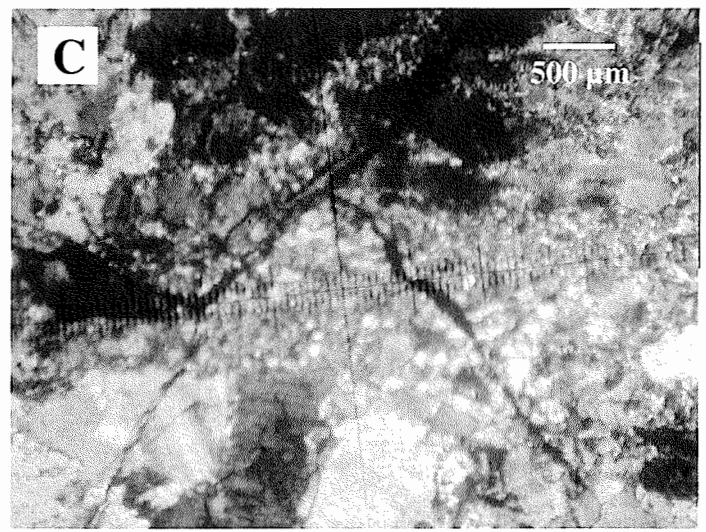

Figure 23c: Thin section of a rock sample taken from the quarry showing abundant quartz and feldspar.

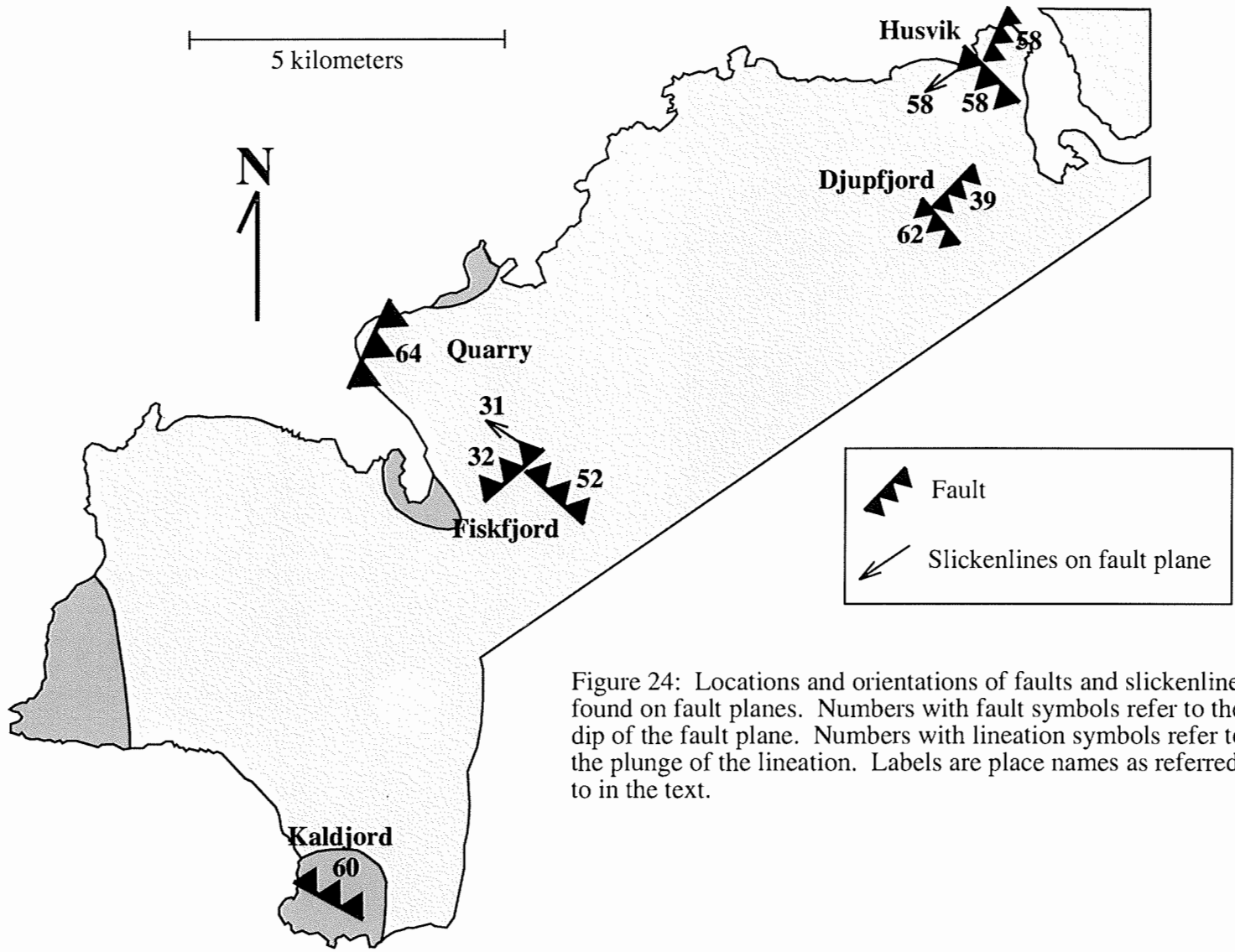

Figure 24: Locations and orientations of faults and slickenlines found on fault planes. Numbers with fault symbols refer to the dip of the fault plane. Numbers with lineation symbols refer to the plunge of the lineation. Labels are place names as referred to in the text.

extensional periods of deformation. Four of the brittle faults are associated with pseudotachylite veins that parallel them.

Two faults occur in the northernmost part of the study area near Husvik (Figures 23 and 24). One is a minor fault oriented 024 58° SE with less than a meter of normal offset in the compositional layering of the migmatitic gneiss, hanging wall-down-to-the-southeast. This fault is vertically traceable only for a few meters in the outcrop at which it is exposed. The other fault is larger and is oriented 315 58° SW. There is a slickenline lineation along the fault plane trending 236 58° (Figure 24). This fault is associated with a meter thick shear zone of the same orientation in the footwall directly beneath the brittle fault plane. Shear sense indicators in the shear zone indicate down-dip normal-slip displacement. There are no offset markers to quantify the amount of displacement along the fault. This fault is traceable between two locations that are approximately 90 meters apart.

In the northeast part of the study area there are two minor faults located on the north side of Djupfjord (Figure 24). They are oriented 320 62° SW and 044 39° SE. These faults are located at outcrops nearly 20 meters away from each other and, thus, they were not observed to intersect. Each was traceable for less than five meters and showed between 40 and 50 centimeters of normal displacement.

In the central part of the study area, close to the coastline, a major, 20-meter thick breccia zone is exposed in a rock quarry (Figure 23). Within this zone, 10- to 20-centimeter thick veins of feldspathic rock are folded and fractured and show normal offset along fracture planes (Figure 23b). Fracture planes are near vertical along the upper quarry walls, but are less steep near the bottom. Orientation near the lower part of

these planes is 025 64° SE. Thin sections of these rocks show highly fractured grains and very thin veins of pseudotachylite (Figure 23c). The zone has been flushed with hydrothermal fluids. There are large amounts of salmon-pink potassium feldspar in the altered areas and the fault surfaces have been epidotized. Although the fault itself is not traceable to other locations because of vegetative cover, evidence of hydrothermal fluids in fractures is visible at outcrops up to 3 kilometers to the north along the strike line of the fault. It is likely that this fault connects directly to one of the several imaged in the directly offshore seismic lines reported by Davidsen and others (2001). The strike orientations are similar and it appears to lie within the hanging wall block to a major detachment imaged in the profile. Sample Q was collected from this quarry and analyzed for $^{40}Ar/^{39}Ar$ isotopes (see below).

Two brittle faults are located southeast of the quarry on the north side of Fiskfjord (Figure 23). The one located more to the west is oriented 049 32° NW. The fault surface is covered by a 5-centimeter thick vein of pseudotachylite, the thickest one observed in this study (Figure 7b), and has a down-dip lineation trending 303 31°. Footwall rocks up to a half-meter thick beneath the fault plane are sheared (Figure 17b). Shear-sense indicators visible at the outcrop scale show normal, hanging wall-to-the-northwest displacement. The entire fault zone is approximately two meters thick and is traceable across the ridge on which it occurs, approximately 500 meters before disappearing beneath a grass and shrub covering. The fault located more to the east (Figure 23) is oriented 312 52° NE and is also coated with a vein of pseudotachylite approximately 3 centimeters thick. There is no indication in the outcroppings of movement sense along

this fault, which is traceable for almost 80 meters up the hillside on which it occurs before disappearing from view beneath vegetative cover.

Another brittle fault was observed in the southernmost part of the study area at Kaldjord where it cuts mangerite (Figure 23). It is oriented 298 60° NE. The plane of this fault is covered with a 3-centimeter thick vein of pseudotachylite. Movement along the fault plane is marked by significant changes in grain size within the rock, from approximately half a centimeter to just over a millimeter. Rotated and displaced markers indicate that movement along the fault was normal, top-to-the-northeast.

Figure 25 is an equal-angle stereogram of all of the observed brittle faults. Hartman's treatment of these data implies a maximum principal stress direction (σ_1) of 358 49°. This suggests that general movement along the northwest-striking faults was normal oblique sinistral and movement along the northeast faults was normal oblique dextral.

Brittle Fractures and Joints

Brittle fractures occur in this area at nearly every outcrop. For this investigation, brittle fractures are fractures that show no evidence for mesoscopic ductile deformation and have little to no displacement (Figure 26). Most are interpreted as tensile or opening fractures. The ones measured and analyzed were those that occurred in sets of approximately the same orientation and, thus, technically are joints (Davis and Reynolds, 1996). Brittle fractures that occur singly may be a result of pressure release due to erosion and, thus, are not tectonic in origin, and so were not analyzed here. Brittle fractures commonly were found within shear zones and had orientations similar to the

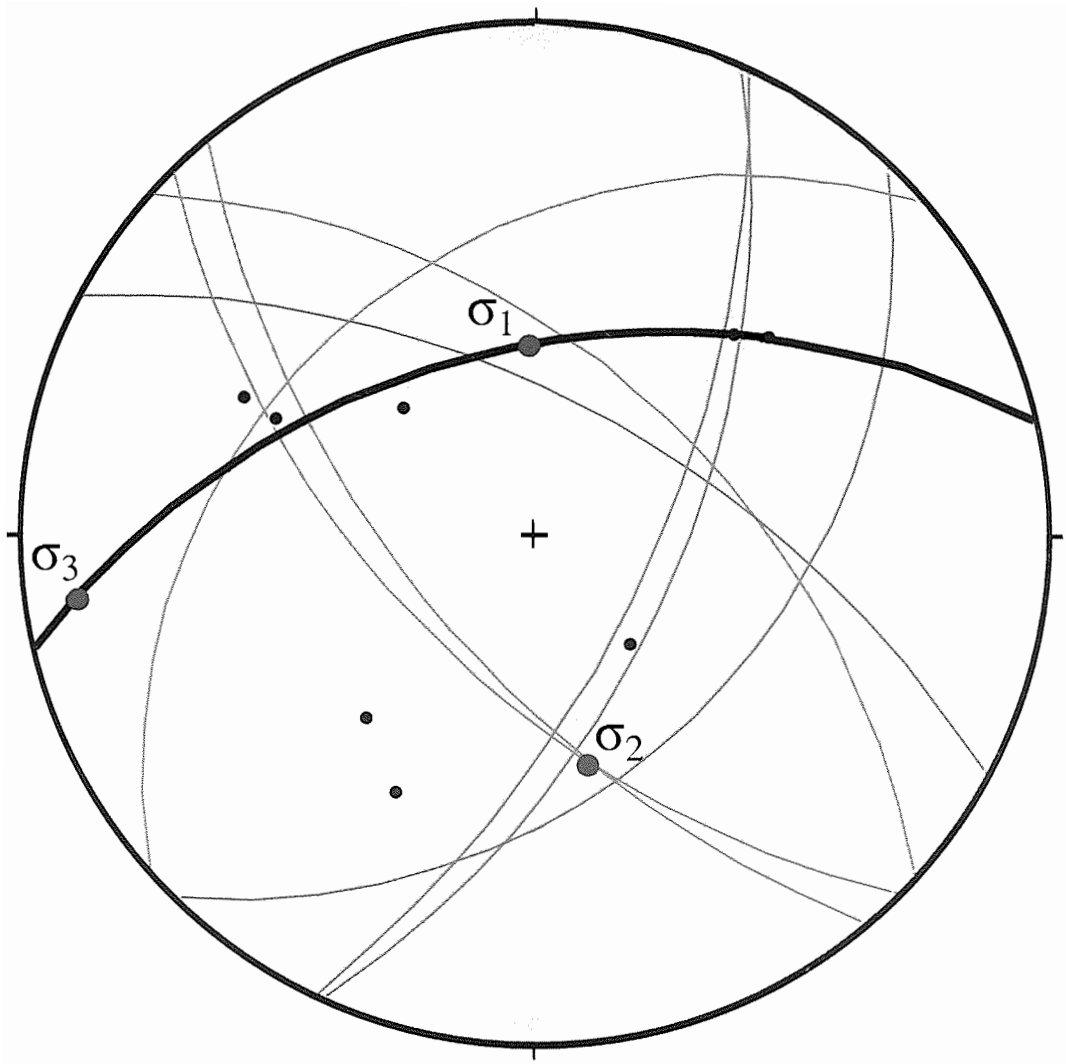

Figure 25: Equal area stereogram of brittle faults in the study area. The green great circles are the fault planes. The black dots are the poles to these planes. The black great circle is the sigma 2 principal plane. Sigma 1, sigma 2, and sigma 3 principal axes are shown by red dots.

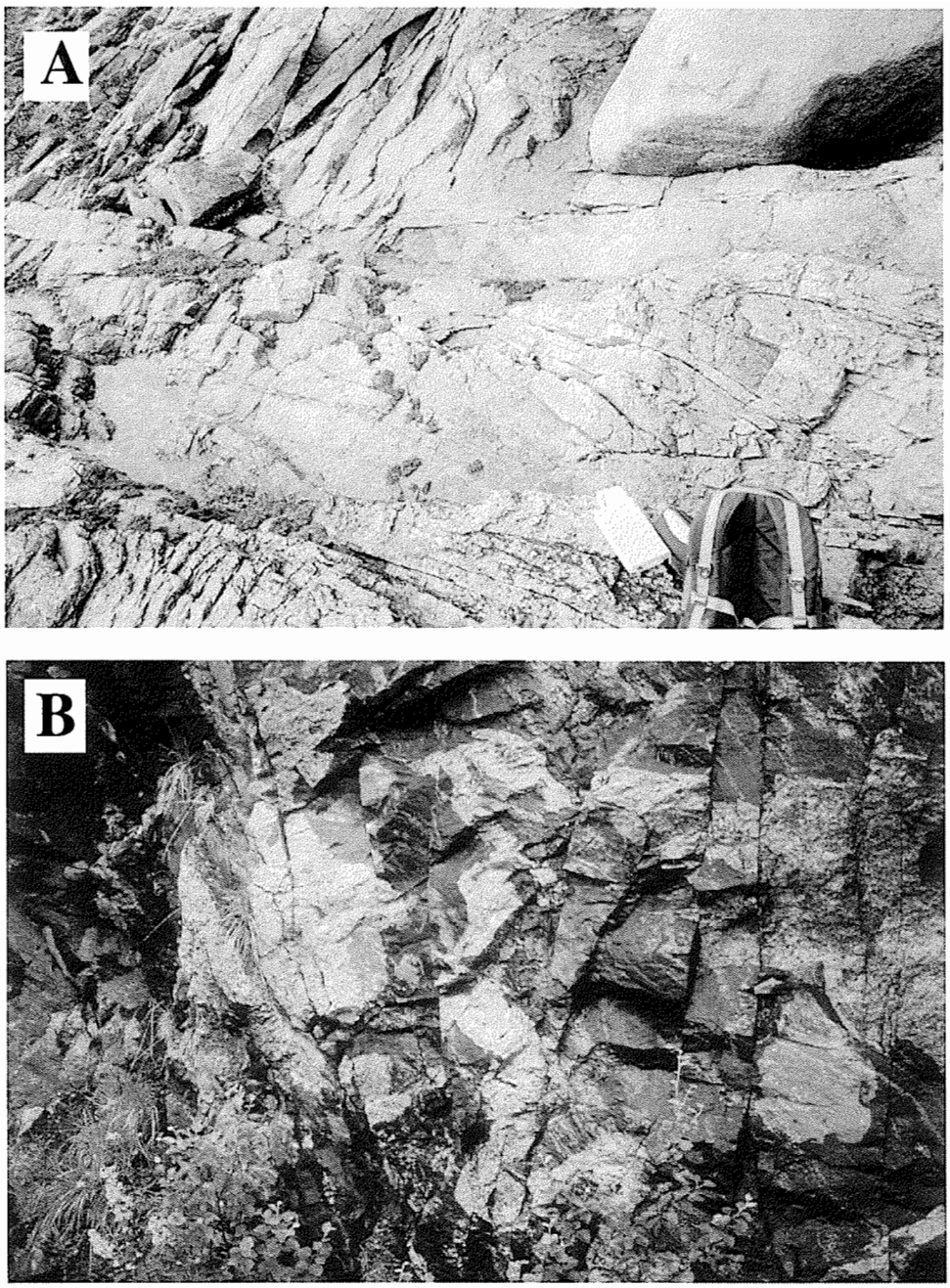

Figure 26: Photographs of brittle fractures. A) Fractures with similar orientations to the shear zone (shear zone located to right of field book). This outcrop contains migmatitic gneiss and is located in the southwest part of the study area just north of Kvitnes. B) Compositional banding, although intensely folded several ways, is not significantly offset by the vertical fractures. This outcrop contains migmatitic gneiss and is located on the north side of Sigarfjord. The view of the photograph is 10 meters across

foliation of the shear zone (Figure 26a). However, the lack of significant displacement along these fractures indicated that the similarity in orientation of the fracturing was due to pressure release having exploited the previously formed foliation and not a result of the same deformation that formed the zone.

Four major sets of brittle fractures are deduced for rocks of the study area (Figure 12d); their orientations are 280 80° S, 355 85° E, 020 90°, and 065 90°. The fact that these structures are still subvertical probably indicates that there has been very little rotation or movement since they were formed. Hartman's treatment using the equal-angle stereogram in Figure 27 indicates that these major sets of fractures had a σ_1 oriented 316 6°. The extensional stresses that caused these would have been oriented in a near horizontal northwest-southeast direction, approximately 315/135.

Dividing the study area into subareas does not allow many smaller patterns to emerge from the data collected on the brittle fractures (Figure 28). There are major sets in subareas A and B, but these roughly coincide with marginal rocks for major faults in the area. Other subareas have relatively scattered point maxima or great circle spreads on their stereograms. More information seems to be gained by viewing the brittle fractures over the entire scale of the study area in this case (i.e., Figure 12d).

Pseudotachylites

Pseudotachylites are unusually common in the study area and are found associated with many different types of structures. Typically, these rocks are thought to be formed by frictional melting from heat emitted during brittle fracturing associated with faulting. They generally occur in the study area as planar, tabular features that are

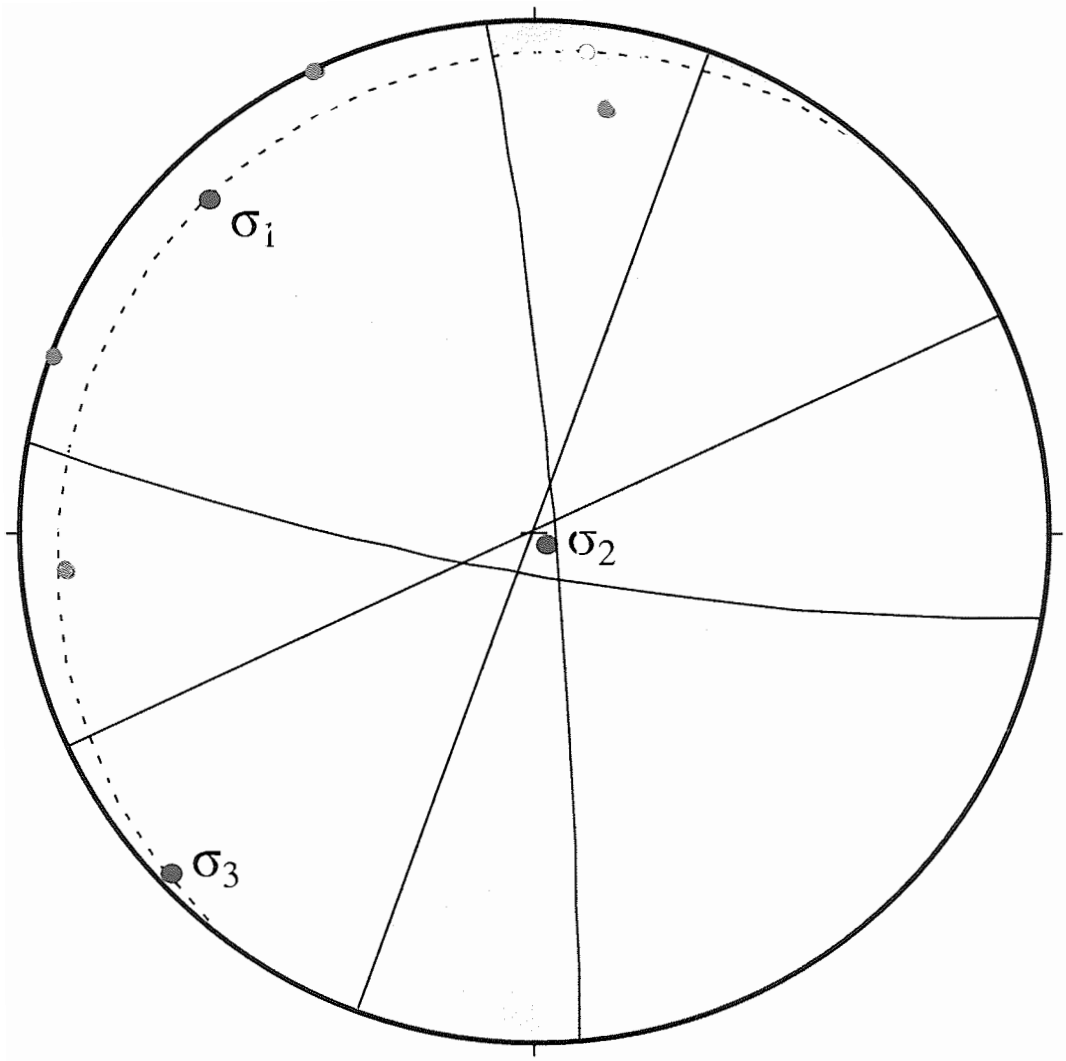

Figure 27: Equal angle stereogram showing Hartman's treatment of the four major sets of brittle fractures. Black great circles are the planes of the major brittle fracture sets (see Figure 12d). Green dots are the poles to these planes. Red dots indicate the orientations of principal strain axes sigma 1, sigma 2, and sigma 3. The great circle is the sigma 2 principal plane.

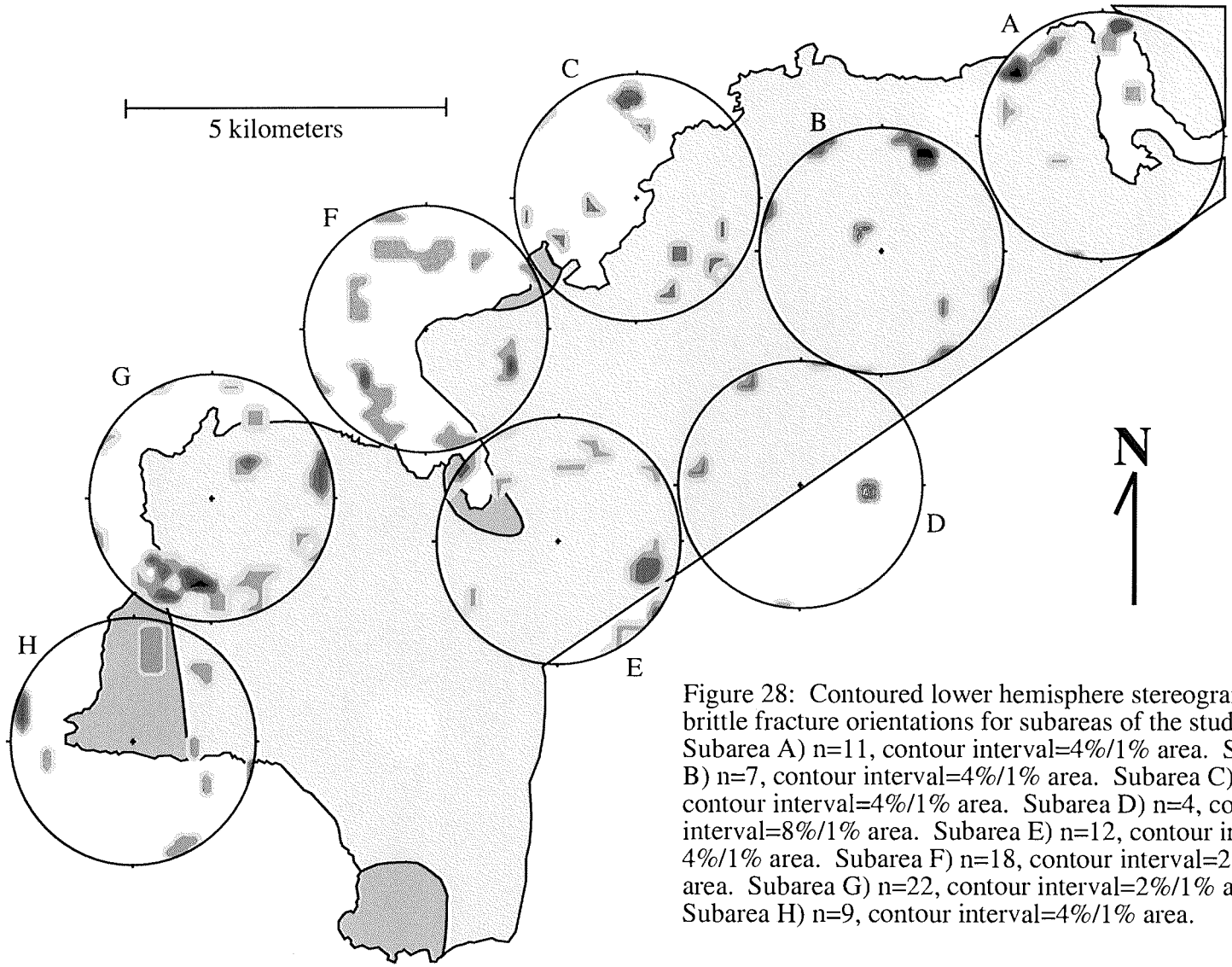

Figure 28: Contoured lower hemisphere stereograms of brittle fracture orientations for subareas of the study area. Subarea A) n=11, contour interval=4%/1% area. Subarea B) n=7, contour interval=4%/1% area. Subarea C) n=11, contour interval=4%/1% area. Subarea D) n=4, contour interval=8%/1% area. Subarea E) n=12, contour interval= 4%/1% area. Subarea F) n=18, contour interval=2%/1% area. Subarea G) n=22, contour interval=2%/1% area. Subarea H) n=9, contour interval=4%/1% area.

commonly oriented along the fault plane or wispy, wedge-shaped features branching off of it. Along the fault plane, pseudotachylite is usually 3 to 5 centimeters thick. The offshoots are typically thinner, splay off in various directions, and thin out as they terminate. They are opaque, black, extremely fine-grained rocks. In thin section the pseudotachylites appear as veins of very fine-grained material (glass or microlites) that is indeterminate using standard petrographic microscopy. There are frequent clasts of host rock included within the pseudotachylite veins.

In the study area, pseudotachylites are found along brittle faults, on the shoulders of shear zones, and associated with brittle fractures. In the case of brittle faults, pseudotachylites commonly occur directly on the fault plane, indicating they were formed simultaneously with movement along the fault. Where pseudotachylite occurs within shear zones, it is sheared along with the zone and is never found to truncate or cross cut the zone. Commonly, pseudotachylites occur on the planes of brittle fractures, suggesting they may have formed simultaneously, or that the fracture may have occurred as a result of the injection of the pseudotachylite. In some cases pseudotachylite veins fill fractures oriented parallel to the fracture sets. Rarely, some pseudotachylites were found isolated from these structures or other pseudotachylites. These were most likely offshoots of nearby structures that were not exposed. At some outcrops the pseudotachylites are folded, fractured, or sheared (Figure 7), indicating that they were part of earlier, rather than later deformation.

The stereogram depicting pseudotachylite orientations for the entire study area has a scattering of points most with moderate to steep dips (Figure 12e). Stereograms for subareas of the study area show similar distributions (Figure 29). This type of geometric

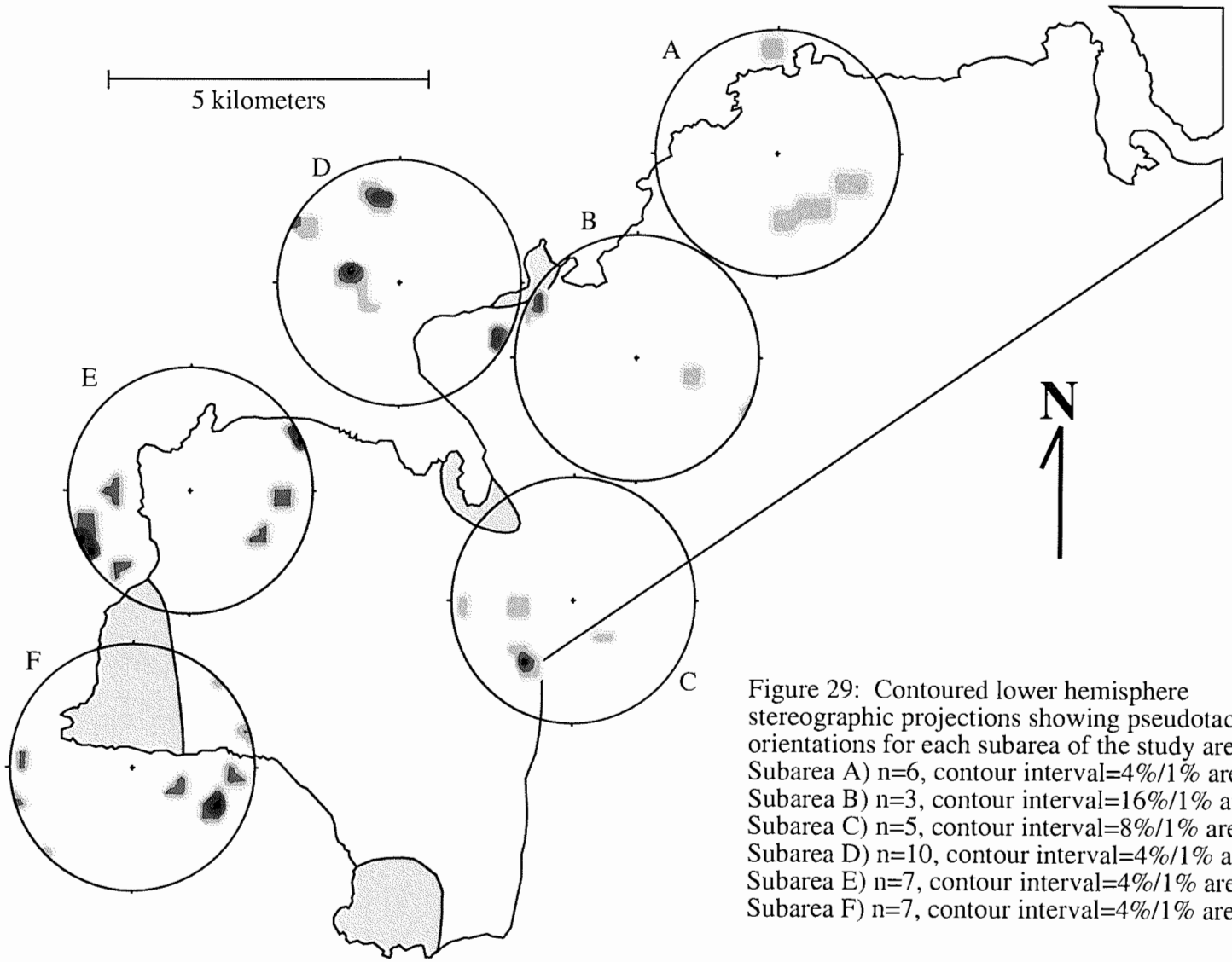

Figure 29: Contoured lower hemisphere stereographic projections showing pseudotachylite orientations for each subarea of the study area. Subarea A) n=6, contour interval=4%/1% area. Subarea B) n=3, contour interval=16%/1% area. Subarea C) n=5, contour interval=8%/1% area. Subarea D) n=10, contour interval=4%/1% area. Subarea E) n=7, contour interval=4%/1% area. Subarea F) n=7, contour interval=4%/1% area.

analysis of pseudotachylites may not be useful due to the somewhat random orientations of the smaller offshoots from the main pseudotachylite vein. A more meaningful analysis would require differentiating the main pseudotachylite veins from the smaller offshoots, which, unfortunately, is not possible given the data collected during this study.

$^{40}AR/^{39}AR$ ISOTOPIC ANALYSIS AND INTERPRETATIONS

Eight samples were selected and submitted for $^{40}Ar/^{39}Ar$ isotopic analysis in the U.S. Geological Survey geochronologic facility in Denver, Colorado, under the direction of Mr. M. Kunk. These samples contained a significant amount of muscovite and, in some cases, potassium feldspar, both of which were separated and analyzed using the step-heating method (see Steltenpohl and Kunk, 1993, for methodology and references). All of these samples were from shear zones or faults or from their shoulder/country rocks from different parts of the study area (Figure 30). Most workers generally report that the closure temperature for retention of ^{40}Ar in muscovite is ~350°C (Purdy and Jäger, 1976; Cliff and Cohen, 1980; Harrison and McDougall, 1981). The closure temperature for potassium feldspar is not a unique value. Potassium feldspar spectra commonly are discordant and interpreted to reflect diffusion gradients formed during cooling. K-feldspar profiles determined in this study are diffusional, and the minimum age heating steps are interpreted to reflect cooling through roughly ~250°C, which generally is compatible with studies reported by Harrison and McDougall (1982) and Harrison and Be (1983). Three biotite concentrates also were analyzed but these yielded ages older than muscovite dated from the same specimen, implying geologically meaningless ages, probably due to incorporation of extraneous ^{40}Ar. One of the biotite samples was from

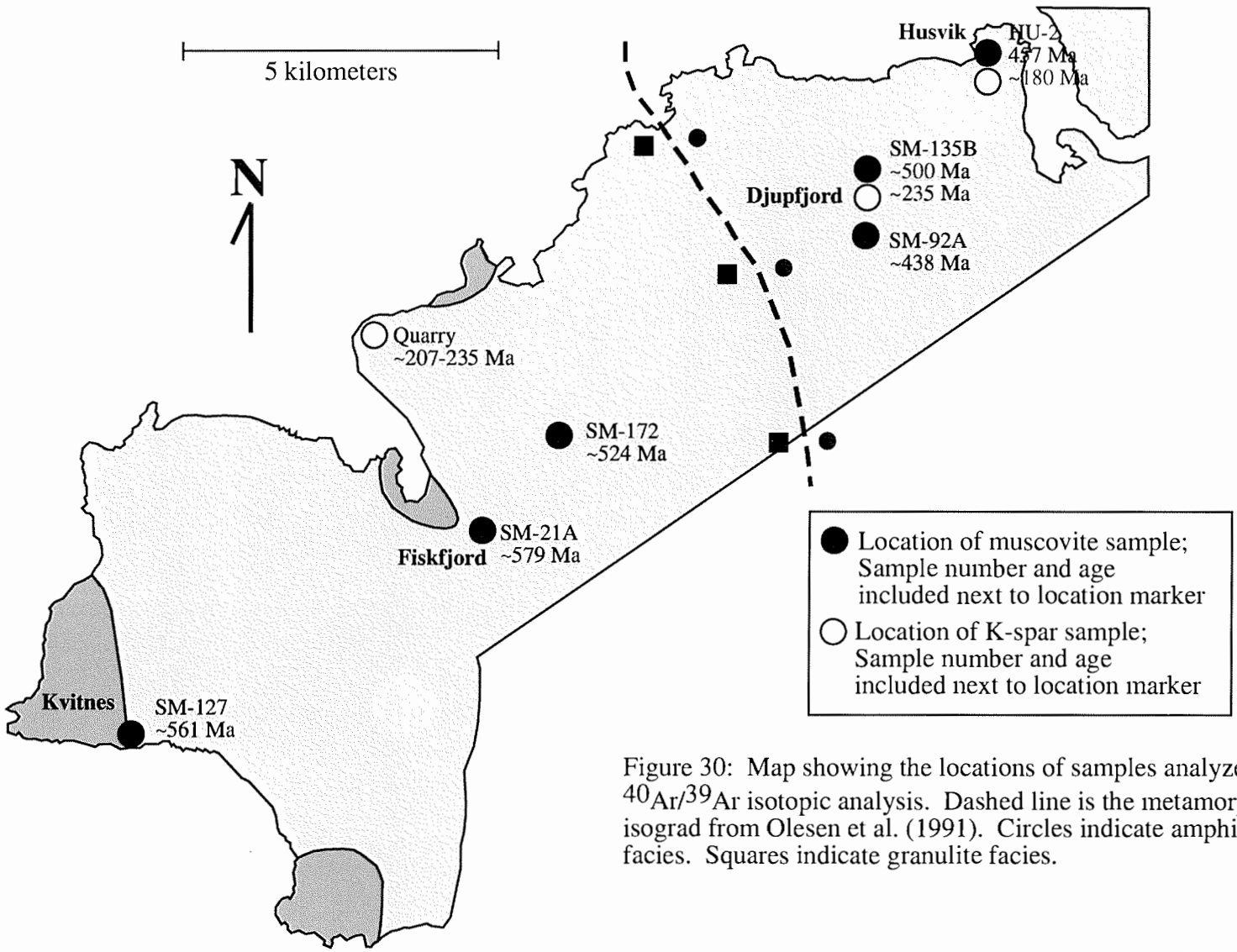

Figure 30: Map showing the locations of samples analyzed in $^{40}Ar/^{39}Ar$ isotopic analysis. Dashed line is the metamorphic isograd from Olesen et al. (1991). Circles indicate amphibolite facies. Squares indicate granulite facies.

the dolerite intrusion described above in the section on lithology. Tabulated results of the analyses are listed in the appendix.

Muscovite Analyses

Most of the muscovite profiles are complex, with only one yielding a plateau age (Fleck, et al., 1977)(HU-2)(i.e. Figure 31) for the six muscovite samples analyzed. The general age range is between ~450 and 590 Ma. Sample SM-21A is from the migmatitic gneiss directly southeast of Fiskfjord (Figure 30). The sample was collected less than a meter from a northwest-striking shear zone. The muscovite grains ranged in size from 0.02 to 0.025 millimeters and form the gneissic foliation rather than a deformed remnant of that fabric. The spectrum for SM-21A has a hump throughout the first half of the heating steps, climbing to ~590 Ma and then descending to ~550 Ma before gradually stepping back up to 590 Ma. There is a sympathetic relationship between K/Ca and heating-step age, which may indicate compositional control, perhaps by tiny inclusions within the grains. Ignoring the first step (only 0.4% total ^{39}Ar and 75.3 radiogenic yield) yields a range from ~460 Ma to 590 Ma; the total gas age is ~574 Ma (Figure 31).

Muscovite sample SM-127 is from a schistosity-forming population separated from a schist sample collected from the migmatitic gneiss complex along the shoreline south of Kvitnes (Figure 30). This sample was located near a minor, localized, northeast-striking shear zone, but there was no microstructural indication to suggest that the muscovite experienced any strain related to this zone. Muscovite is idioblastic and ranges from 0.2 to 0.75 millimeters in length. The age spectrum for SM-127 has two humps, both with maximum ages at ~580 Ma. Disregarding the first step (only 0.4% total

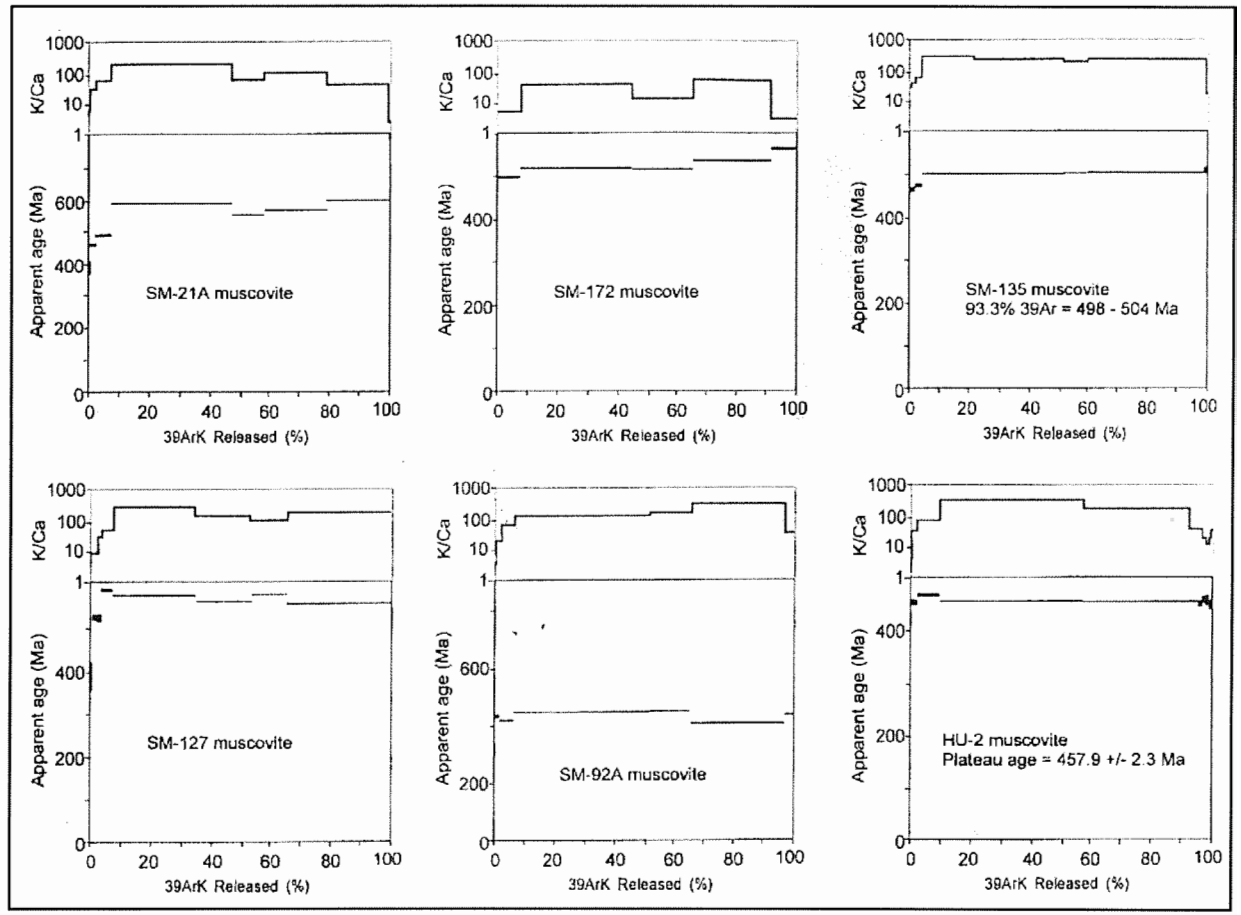

Figure 31: $^{40}Ar/^{39}Ar$ step-heating release spectrum for muscovite samples.

^{39}Ar and 59.5 radiogenic yield) the range of ages is ~522 - 585 Ma; the total gas age is ~561 Ma (Figure 31).

Muscovite sample SM-172 was taken from a migmatitic gneiss less than a meter from a northeast-striking shear zone associated with the faults along Fiskfjord (Figure 30). Thin section analysis indicates that the muscovite from this sample ranges from 0.07 to 0.43 millimeters in length and forms the schistosity. The smaller grains commonly are 'peels' that have fish or phacoidal shape and are clearly derived through post-crystallization shearing of the larger grains. The age release spectrum for SM-172 has a similar architecture (i.e. a single hump) and slightly younger age range (~501 - 561 Ma) to that of SM-21A; total gas age is ~524 Ma (Figure 31).

Sample SM-92A was taken less than a meter from a northeast-striking shear zone located just northeast of Djupfjord (Figure 30). This rock is a feldspathic schist from the migmatitic gneiss complex, and it contains sparse, fine-grained 0.03 millimeter muscovite. Again, the age spectrum has a weak, single-hump architecture, with ages ranging from 434 to 454 Ma (disregarding the first two and last steps, which together account for only 1% ^{39}Ar with relatively lower radiogenic yields); the total gas age is 438 Ma (Figure 31).

Sample HU-2 was collected less than a meter from the northwest-striking shear zone within the footwall of the major subhorizontal shear zone depicted on Løseth and Tveten's (1996) map (Figure 32) at Husvik (Figure 30). This migmatitic rock has biotite-feldspar schist melosomes mixed with muscovite-biotite pegmatitic leucosomes. Muscovite from the leucosomes are up to one centimeter in length, are not deformed, and

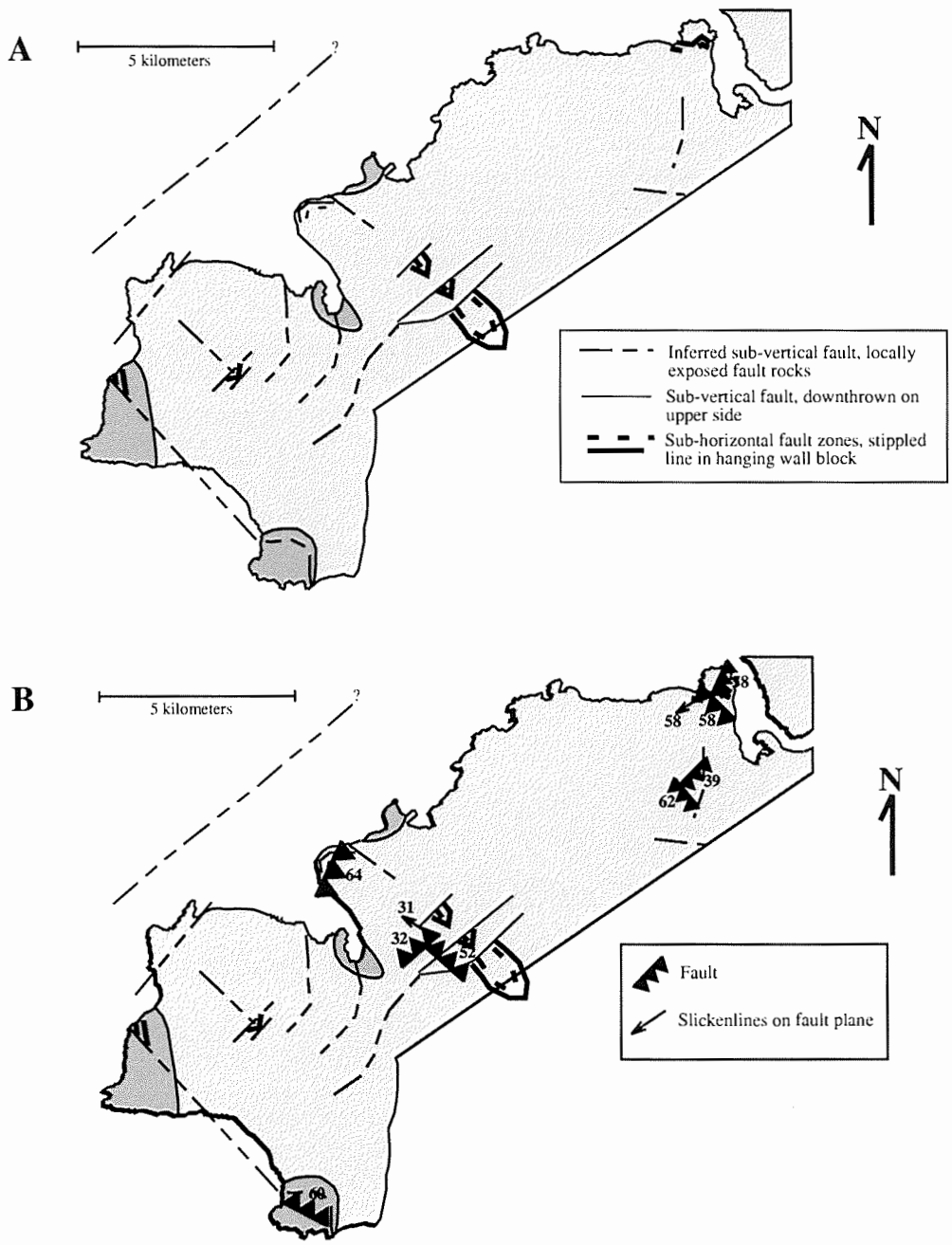

Figure 32: A) Structural map of the study area modified from Løseth and Tveten (1996). B) Comparison of the brittle faults found in the study area to the faults described by Løseth and Tveten (1996).

define the schistosity. The 456.9 ± 2 Ma age is the only plateau recorded by any of the analyzed specimens (Figure 31).

Sample SM-135B was collected near a northwest-striking shear zone located on a prominent ridge north of Djupfjord (Figure 30). This shear zone is oriented 336 18° SW. Its orientation and location imply an association with the northwest-striking Djupfjord fault that is located less than 200 meters north on the opposite ridge. This rock is a migmatitic gneiss and muscovite from it ranged from 0.1 to 1.0 millimeters in length and helped define the gneissosity. The muscovite grains are thin peels and fish derived from larger muscovites in the shoulder rocks of the shear zones. The age-release profile is relatively flat coming very close to a plateau. Steps 4 through 7 contain 93.3% of the total ^{39}Ar released, each step having radiogenic yields of 98.9 or higher, and ages range from 498 to 504 Ma; total gas age is ~500 Ma (Figure 31).

Potassium Feldspar Analysis

Samples SM-135B and HU-2 also contained potassium feldspar that was separated and analyzed for $^{40}Ar/^{39}Ar$ isotopes (Figure 33). Potassium feldspar from SM-135B was up to 0.75 millimeters in length and flattened parallel to the gneissosity. Potassium feldspar from HU-2 was up to 4 millimeters in length and contained numerous sericite inclusions and tartan twin planes. Both analyses resulted in similar diffusional-release profiles. The diffusional gradient for SM-135B has a maximum age step of ~460 Ma and a minimum at ~235 Ma; Hu-2 was ~438 and ~180 Ma, respectively (Figure 33).

Sample Q was taken from the quarry within the major fault that cuts the migmatitic gneiss complex near the west-central shoreline (Figure 30). Potassium

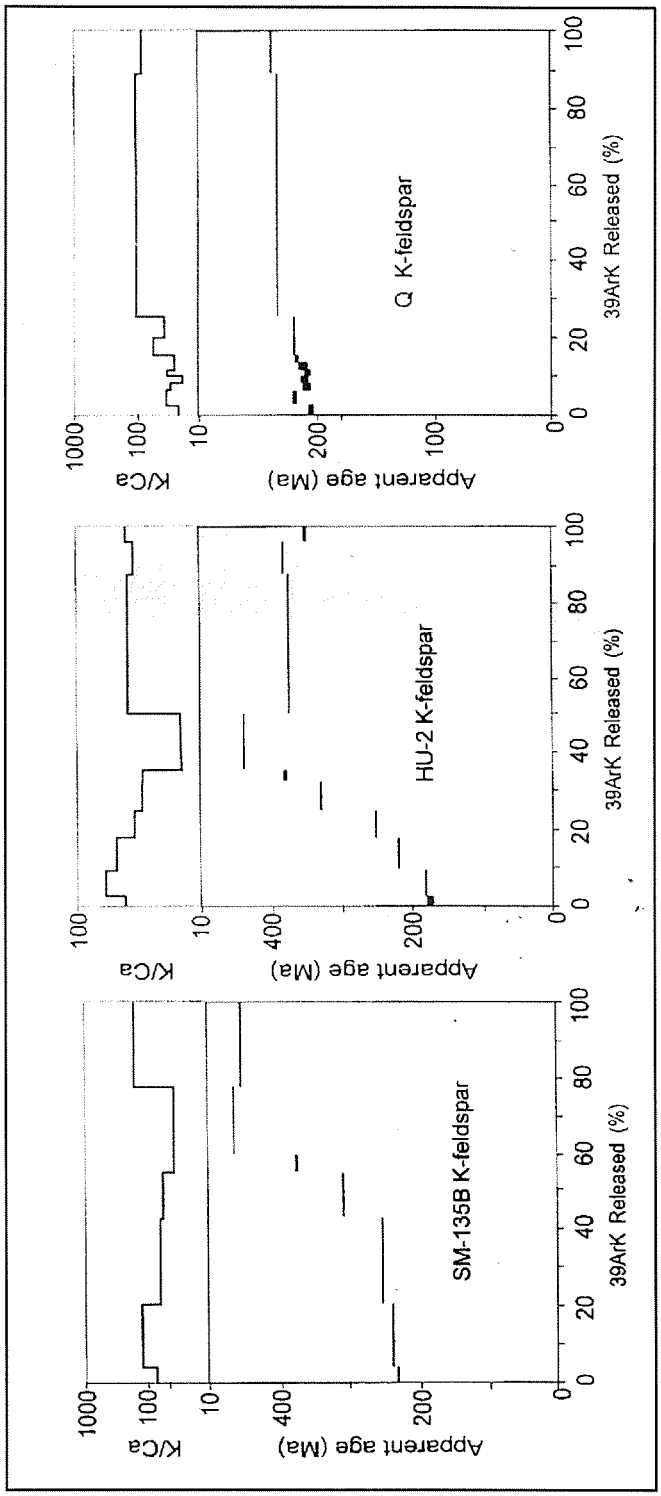

Figure 33: $^{40}Ar/^{39}Ar$ step-heating relative spectra for potassium feldspar samples.

feldspar from this sample was up to 1 centimeter in diameter, broken and veined, and salmon-pink colored, the result of the flushing of the zone by hot, hydrothermal fluids associated with faulting. This release profile also is diffusional but its age distribution is much more condensed in than the other analyses; the maximum age step is 239 Ma and the minimum is ~207 Ma (Figure 33).

Interpretation of $^{40}Ar/^{39}Ar$ Results

The complex architecture of the muscovite $^{40}Ar/^{39}Ar$ spectra make it difficult to pin down a precise, detailed cooling history for rocks in the study area. The most general conclusion that can be drawn, however, is that these rocks record cooling through the ~350° C isotherm during the Cambro-Ordovician; that is, sometime after ca. 570 and before ca. 440 Ma. This is surprising since these rocks had been argued to have "escaped" Caledonian deformation and metamorphism (Griffin et al., 1978). This interpretation has significant implications for tectonic evolution in this region that are addressed in the Discussion section, below.

The potassium feldspar results document a pulse, or multiple pulses, of uplift and cooling between ca. 235 Ma and 185 Ma. This timing is consistent with extensional faulting that produced basins filled with Triassic-Jurassic sediments flanking various parts of the Lofoten Ridge (see Steltenpohl et al., 2004).

DISCUSSION

Since the 1970's, various workers have been engaged in characterizing a geotectonic transect across the Scandinavian Caledonides along latitude 68.5° North (Figure 34). This world class transect progressively traces the Baltic basement-cover contact, from east to west, from the unmetamorphosed and undeformed nonconformity in the Swedish foreland (Bax, 1986, 1989), to biotite- and garnet-zone thrusts in the external Rombak window (Hodges, 1982; Crowley, 1985; Tull et al., 1985) to the kyanite-zone shear zone with the internal Western Gneiss basement complex (Hodges at al., 1982; Andresen and Steltenpohl, 1991) (Figure 34). Observations from this eastern half of the transect supplied key elements used by Hodges and others (1982) to formulate their A-type subduction zone model that has driven tectonic interpretations over the past twenty years. Their model purported that relations along this transect reflect intermediate crustal depths (30 km or deeper) for formation of the ancient, Scandian (Silurian) continent-continent subduction zone boundary. In the A-type model, as the Baltic margin was subducted westward beneath Laurentia, Scandian basement-involved thrusts developed progressively toward the foreland in a fashion similar to a piggyback style, foreland-fold-and-thrust belt.

The western end of this part of the transect presented problems for the A-type model where it approached the boundary within the Lofoten basement (see near the "H" in Figure 34) directly east of the study area (e.g., Bjørklund, 1987). Despite its most

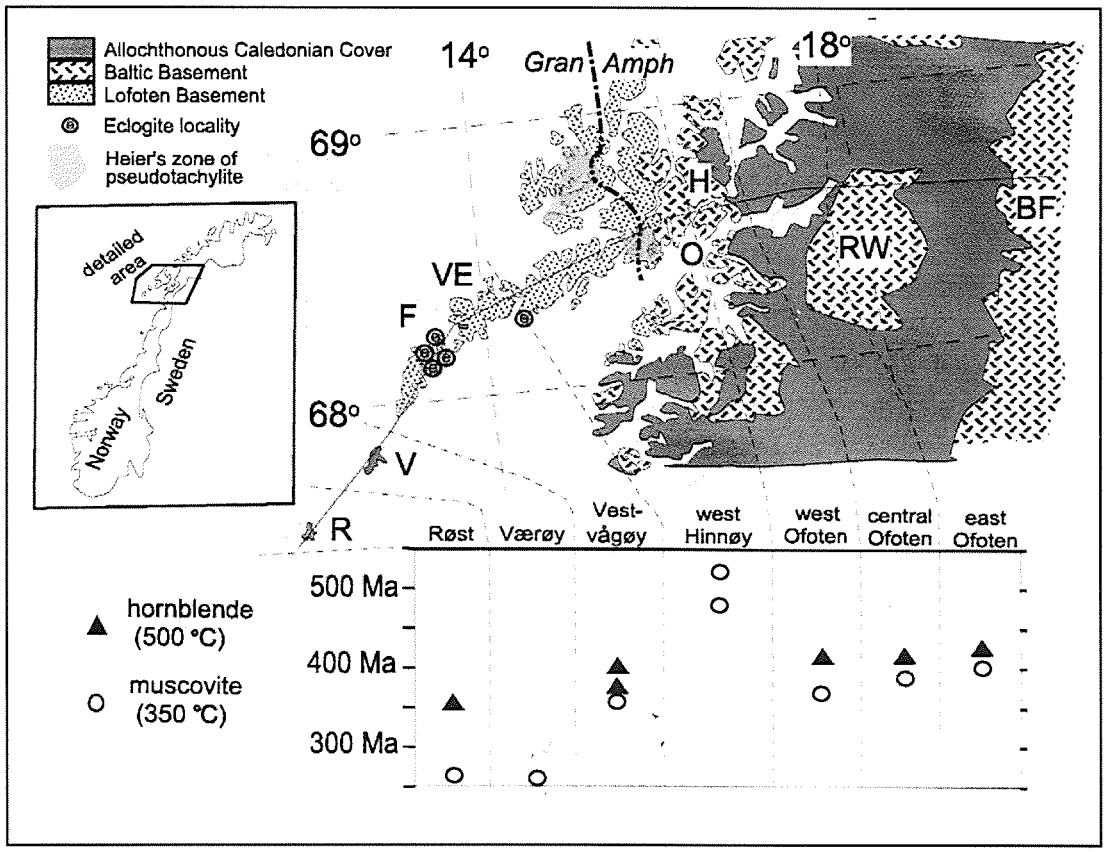

Figure 34: Compiled map along the geotectonic transect across the Scandinavian Caledonide Orogen. Figure compiled from Bax (1986, 1989), Hodges (1982), Hodges and others (1982), Crowley (1985), Tull and others (1985), and Andresen and Steltenpohl (1991). F = Flakstadøy, H = Hinnøy, O = Ofotfjord, BF = Baltic Foreland, RW = Rombak Window, VE = Vestvågøy, V = Våerøy, R = Røst, Gran = Granulite facies, Amph = Amphibolite facies, dot-dashed line = curved discontinuity

internal position within the very core of the palinspastically restored orogen, field and petrologic evidence indicated that Lofoten had occupied a high crustal level throughout the Caledonian orogeny, having totally "escaped Caledonian metamorphism and deformation" (Griffin et al., 1978). Hakkinen (1977) and Tull (1977) found Caledonian structures and fabrics to disappear structurally downward, over a distance of ~250 m, into the basement in this area. The same workers hypothesized that Lofoten might be a "microcontinental fragment" that had originated between Greenland and Norway, and that late-Caledonian nappes were emplaced due to its beaching upon the Baltic margin. Alternatively, Bartley (1982) hypothesized that the lack of Caledonian deformation and metamorphism in Lofoten might be due to the limited availability of fluids to these dry, granulite-facies protoliths. The basal Caledonian thrust, therefore, was interpreted to have passed over the top of Lofoten, and it was considered to be the westward continuation of the old Scandian subduction zone boundary (Hodges et al., 1982).

In the mid-1990's, researchers found a rich and diverse history of Caledonian metamorphism and deformation (Hames and Andresen, 1996; Klein et al., 1999; Steltenpohl et al., 2004) within klippen of metasedimentary rocks of southwest Lofoten, called the "Leknes group" (Tull, 1977). These structures and fabrics disappear structurally downward in accord with Bartley's (1982) model of limited basement involvement. Recently, Steltenpohl and others (2003) documented that the intense, moderately high-pressure, amphibolite-facies metamorphism of the Leknes group was not related to a Proterozoic event (i.e., the "Leknes event" of Griffin et al., 1978, and Tull, 1977) but rather occurred during the Caledonian (Holloman, 1996; Mooney, 1997; Waltman, 1997; Klein and Steltenpohl, 1999; Klein et al., 1999; Hames and Andresen,

1996; Steltenpohl et al., 2004). Klein and others (1999) and Steltenpohl and others (2004) concurred that Lofoten was the westward, more deeply subducted continuation of the Baltic margin.

Coker and others (1995) discovered that $^{40}Ar/^{39}Ar$ hornblende and muscovite dates from the Caledonian nappes across Ofoten are progressively younger towards Hinnøy. The same authors hypothesized that this pattern resulted from hinged-to-the-east isostatic adjustment and exhumation along a west-dipping, crustal-scale extensional fault that possibly is "covered by young sediments along the modern continental shelf." More recent work in Lofoten (Hames and Andresen, 1996; Steltenpohl et al., 2004) documents continuation of this same pattern southwestward across the Lofoten archipelago. Klein and others (1999) couched structures and mineral cooling dates from Vestvågøy in terms of documenting continuity of the Scandian A-type subduction zone through these exposures. The A-type model appears to be challenged by the Cambro-Ordovician muscovites from this study (Figure 34). The new Cambro-Ordovician muscovite dates from rocks in this study, however, present a distinct older-age anomaly in west Hinnøy (Figure 34).

Two possible scenarios, one structural and the other inferred from thermal histories, might account for both the relationship depicted in Figure 34 and the geology. First, a structural break in west Hinnøy may separate crustal blocks, one metamorphosed and deformed in the Ordovician and the other in the Siluro-Devonian. A structural explanation could lie in either of two known structures in west Hinnøy, the Austerfjord thrust (Hakkinen, 1977) and the Gullesfjord shear zone (Griffin et al., 1978; Hakkinen, 1977). The Austerfjord thrust originally was suggested to be the suture between Lofoten

and Baltica (Hakkinen, 1977; Tull, 1977) before Bartley (1981; see also Hodges et al., 1982) argued, on structural and fabric grounds, that it was the isoclinally folded continuation of the basal Caledonian thrust to the east. However, more recent mapping and structural studies by Rykkelid (1992) indicate that the Austerfjord and a previously unrecognized thrust, the Tjeldøy thrust, imbricate, rather than fold, the basal Caledonian thrust. These thrusts carry slabs of basement and attached cover and project into large-scale (>10 km amplitude) basement-cored recumbent fold nappes reported by Bartley (1981) and Steltenpohl (1987) on eastern Hinnøy and farther east in Ofoten. Interestingly, Rykkelid (1992, Figure 15, cross section A) shows these basement-cover imbricates and their thrusts to roll over directly west of Austerfjord and to root steeply into the poorly known Gullesfjord shear zone (Griffin et al., 1978; Hakkinen, 1977). Also significant is Rykkelid's suggestion (Rykkelid, 1992, Figure 15) that an east-dipping, tops-east, ductile extensional shear zone is contained within the Gullesfjord zone. Future studies aimed at understanding the development of the Austerfjord and the Gullesfjord shear zones may provide information supporting or refuting this interpretation.

Alternatively, the Cambrian-Ordovician dates from the present study might reflect partial to complete resetting of the $^{40}Ar/^{39}Ar$ isotopes in pre-Ordovician muscovites. Recent work by Steltenpohl and others (2003) to date hornblende associated with eclogite shear zones shows that Caledonian metamorphism is profoundly evident in some parts of the basement of western Lofoten. The Caledonian effects on the basement of more central and eastern parts of Lofoten is less clear, however, because previous work (Hames and Andresen, 1996; Klein et al., 1999; Steltenpohl et al., 2004) has focused on

characterization of metamorphism in the Leknes Group. The Cambro-Ordovician muscovites in this study came from what are interpreted as Precambrian orthogneisses and migmatites and no isotopic dates are reported on any unit in the study area. However, muscovite-bearing gneisses of western Hinnøy are fairly typical of the correlated basement lithologies in central Lofoten. Thus, these dates from the shear zones and aluminous gneisses from the study area on western Hinnøy may provide compelling evidence that the main Caledonian effects in central Lofoten were limited and that a record of pre-Silurian metamorphism (albeit partially 'reset') is preserved.

Another potentially important implication of the present study relates to the apparent smooth progression of metamorphism westward across Ofoten that continues through the amphibolite/granulite isograd in the study area to its last exposed vestiges as eclogite-facies rocks in western Lofoten. As described earlier, both the eclogite- and granulite-facies metamorphism in this region had previously been interpreted as having resulted from Proterozoic events (Griffin et al., 1978; Markl and Bucher, 1997) unrelated to the Caledonian. The discovery that the Lofoten eclogites could have formed as late as 433 Ma (Steltenpohl et al., 2003) combines with these early Caledonian muscovite dates to suggest that these lower-crustal rocks may be a partially intact Caledonian crustal column. Furthermore, ongoing work seems to make it more and more apparent that parts of Lofoten contain Ordovician relics that do not easily fit in the context of existing tectonic models. Corfu (2004) recently dated metatonalite dikes and veins within rocks of the Leknes Group at 469±3 Ma and fabric-forming titanite from the country rock at 461±1 Ma. Likewise, paleomagnetic studies on pseudotachylite collected from Heier's Zone of Pseudotachylites (Heier, 1960) are interpreted to suggest Ordovician seismic

faulting (Olesen et al., 1997). Future studies need to be directed at dating metamorphic and deformational features in Lofoten to explore its Caledonian history and clarify its tectonic evolution.

The K-feldspar dates from the present study have significance for the timing and style of post-Caledonian extension along the Norwegian shelf. The various faults and crystal-brittle shear zones in the study area are most probably associated with Triassic-Jurassic extension. In addition to its compatibility with the timing of sediment accumulation in extensional basins flanking the Lofoten and associated basement ridges, this timing also is consistent with $^{40}Ar/^{39}Ar$ dating of sediments retrieved from cores along the shelf (Sherlock, 2001) as well as argon dating of footwall bedrock units exposed along coastal Lofoten (Hames and Andresen, 1997; Steltenpohl et al., 2004) and the mainland (Carter, 2000; Zeltner, 2001). This timing is consistent with the interpretation of Davidsen and other's (2001) for Jurassic extension based on the discovery of boulders containing Jurassic fossils that have washed up along shore in the present study area.

The K-feldspar dates conflict, however, with Markl's (1998) and Plattner and others (2003) interpretations that all the pseudotachylites in the area are late-Caledonian because they are associated with structures that are formed both during pre- and post-Caledonian times. The assumption being made here is that all of the pseudotachylites in the area are within Heier's Zone of Pseudotachylites and they all formed at about the same time. However, those that are associated with the Eidsfjord thrust may be late-Caledonian, those that are associated with the Jurassic age structures are post-Caledonian, and those associated with Ordovician age structures are early-Caledonian.

Kinematic studies in the area show mainly tops-to-the-west extension, as determined using oriented thin sections containing shear sense indicators (Figure 17). These analyses would indicate a series of west-dipping normal faults that project off shore like those imaged by Davidsen and others (2001). This series of normal faults does not support contractional movement as was suggested by both Markl (1998) and Plattner and others (2003) for motion on the Eidsfjord fault, indicating that it is most likely not related to the normal faults in the study area.

When compared with findings by Løseth and Tveten (1996) the structures in this study area show similarities in location but not extent (Figure 32). In some cases Løseth and Tveten (1996) present kinematic interpretations and greater strike lengths of faults where no evidence to support such findings was found during this study. Løseth and Tveten (1996) also referred to some structures as faults where, in the field, they appeared as small isolated shear zones (Figure 32). For example, in the very southwest part of the study area there was evidence of a fault at Kaldjord (Figures 24 and 32b). Løseth and Tveten (1996) project this fault several hundred meters to the northwest (Figure 32). In this part of the study area there was evidence of some smaller shear zones (Figure 18), but due to their narrow thickness, visible extent, and orientations they did not seem to be related to the fault at Kaldjord. The data set presented in this study shows two sets of shear zones, one striking northeast and the other striking northwest. A number of the northwest-striking shear zones have very steep dips and elongation lineations that are sub-parallel to strike, indicating oblique, strike-slip movement. Most of the northeast-striking shear zones have shallower dips and slip lines that indicate normal dip-slip movement. Several of these shear zones from both sets coincide with the locations of

some of Løseth and Tveten's (1996) inferred faults (Figures 18 and 32). All of the brittle faults in the study area coincide with faults presented on the map by Løseth and Tveten (1996) (Figure 32b). When comparing the two studies, Løseth and Tveten (1996) extended their findings based on topography and inferred evidence. This study provides direct field observations for locations and orientations of the structures.

CONCLUSION

The plethora of brittle structures exposed in the study area is unusual and likely points to an origin related to some structural anomaly that has not yet been revealed or understood. There are four such potential structural anomalies, some or all of which probably are related, that partly led to the focus of this study: (1) a Jurassic basin postulated by Davidsen and others (2001) to lie directly offshore of the area; (2) Heier's Zone of Pseudotachylite; (3) the Eidsfjord fault; and (4) an extensional detachment that dips toward this area (Steltenpohl et al., 2004). As for (1), the results of this study demonstrate the utility of mapping and analyzing on shore structures for verifying interpretations inferred from offshore seismic studies. The $^{40}Ar/^{39}Ar$ date on K-feldspar from the major 'quarry' fault exposed in the study area, coupled with the kinematic analysis, documents Early Jurassic, normal-slip, tops-west motion. This result is consistent with Davidsen and others' (2001) interpretation for a Jurassic basin lying directly to the west, offshore of the study area. Clearly, the Jurassic was an important period of normal faulting and associated sedimentation in the tectonic development of this region (Steltenpohl et al., 2004).

Heier's Zone of Pseudotachylite, (2), remains an enigma. The presence of microlites and both isotopic and paleomagnetic dates indicate that these pseudotachylites formed during the Caledonian (Løseth and Tveten, 1996; Plattner et al., 2003; Kassos et al., 2004) and, thus, formed earlier and deeper in the crust than did the Jurassic

extensional features investigated. Heier's Zone is indicated on existing maps to form two separate areas; Plattner and others (2003) studied the northwestern area, whereas this study area lies within the southeastern one (Figures 1 and 34). Plattner and others (2003) infer that pseudotachylites in the northwestern area appear to be associated with the immediate hanging wall of the Eidsfjord fault, (3), which they interpret to be an east-directed thrust. The geometric structural analysis of the pseudotachylites did not reveal any kinematic or dynamic trends, which may be due to strong overprinting by the Jurassic extensional event in rocks of the area. No through-going shear zone that might correspond to the Eidsfjord fault was detected. It might be possible, however, that the low-angle mylonitic shear zones in the area are relics of the Eidsfjord fault that has been severely chopped and reoriented by the later, higher crustal-level Jurassic overprint. This is an alluring interpretation because the overall westward sheet-dip of the mylonitic shears also is similar to the Eidsfjord fault. The kinematic analysis for the mylonitic shears, however, indicates tops-west normal slip rather than tops-east thrusting.

With regard to (4), Steltenpohl and others (2004) report evidence for a major Permian extensional detachment in western Lofoten that dips eastward toward the study area. Several of the K-feldspar analyses hint at a Middle Triassic date (235-239 Ma) for rapid uplift/cooling be extensional faulting, and may suggest a link to movement initiated along the Permian detachment toward the west. Although this is a stretch, Carter (2000) also reports $^{40}Ar/^{39}Ar$ and structural evidence for Triassic extension along eastern Vestfjord (Figures 1 and 34).

Ordovician $^{40}Ar/^{39}Ar$ muscovite cooling dates from rocks of the study area are a surprising discovery. These dates are difficult to fit into the tectonic model for combined

A-type subduction with limited basement involvement proposed for this region (e.g., Bartley, 1982, and Hodges and others, 1982). On one hand, they seem to resurrect the notion that Lofoten might be a microcontinent that had beached onto Baltica during the Caledonian Orogeny (Hakkinen, 1977; Tull, 1977). On the other hand, the muscovite dates may record incomplete resetting of older Proterozoic micas such that Lofoten is the westward, lower-crustal continuation of the Baltic margin. Together with its middle- and upper-crustal Baltic basement counterparts preserved toward the east, the orogenic transect from Lofoten to the Swedish foreland may well represent a rare, continuously exposed column through the entire Caledonian continental lithosphere.

REFERENCES

Andresen, A., and Steltenpohl, M. G., 1991, A geotraverse excursion through the Scandinavian Caledonides: Tornetrask-Ofoten-Tromso: International Geologic Correlation Project 233, p. 1.1-6.16.

Bartley, J. M., 1981, Structural Geology, Metamorphism, and Rb/Sr Geochronology of East Hinnøy, North Norway [Ph.D. thesis]: Massachusetts Institute of Technology, Cambridge, Massachusetts, 263 p.

Bartley, J. M., 1982, limited basement involvement in Caledonian deformation, Hinnøy, north Norway, and tectonic implications: Tectonophysics, v. 83, p. 185-203.

Bates, R. L., and Jackson, J. A., 1987, Glossary of Geology, American Geological Institute, Alexandria, Virginia, 3rd ed., 788 p.

Bax, G., 1986, Basement involved Caledonian nappe tectonics in the Swedish part of the Rombak-Sjangeli window: Geologiska Føreningens I Stockholm Førhandlingar, v. 108, p. 268-270.

Bax, G., 1989, Caledonian structural evolution and tectonostratigraphy in the Rombak Sjangeli window and its covering sequence, northern Scandinavian Caledonides: Norges Geologiske Undersøkelse, v. 415, p. 87-104.

Bjørklund, L. J., 1987, Basement-cover relationships and regional correlation of the Caledonian nappes, eastern Hinnøy, N. Norway: Norsk Geologisk Tidsskrift, v. 67, p. 3-14.

Carter, B. T., 2000, Geological investigations in Steigen-Engeløya, north-central Norway (68° N), and their significance for tectonic evolution [M.S. thesis]: Auburn University, Auburn, Alabama, 135 p.

Cliff, R. A., and Cohen, A., 1980, Uranium-lead isotope systematics in a regionally metamorphosed tonalite from the eastern Alps: Earth and Planetary Science Letters, v. 50, p. 211-218.

Coker, J. E., Steltenpohl, M. G., Andresen, A., and Kunk, M. J., 1995, An $^{40}Ar/^{39}Ar$ thermochronology of the Ofoten-Troms region: Implications for terrane amalgamation and extensional collapse of the northern Scandinavian Caledonides: Tectonics, v. 14, no. 2, p. 435-447.

Corfu, F., 2004, U-Pb geochromology of the Leknes Group: an exotic Early-Caledonian metasedimentary assemblage stranded on Lofoten basement, North

Norway: Journal of the Geological Society of London, v. 161, no. 4, p. 619-627.

Crowley, P. D., 1985, The Structural and Metamorphic Evolution of the Sitas Area, Northern Norway [Ph.D. thesis]: Massachusetts Institute of Technology, Cambridge, Massachusetts, 235 p.

Dalland, A., 1975, The Mesozoic rocks of Andøya, northern Norway: Norges geologiske undersøkelse, v. 316, p. 271-287.

Davidsen, B., Smelror, M., and Ottesen, D., 2001, Et nyoppdaget Mesozoisk basseng i Vesterålen: Norsk geologisk tidsskrift foretnigen, Abstracts with Programs, Trondhjeim, Norway.

Davis, G. H., and Reynolds, S. J., 1996, Structural Geology of Rocks and Regions, John Wiley & Sons, Inc., New York, 2nd ed., 776 p.

Fleck, R. J., Sutter, J. F., and Elliot, D. H., 1977, Interpretation of discordant $^{40}Ar/^{39}Ar$ of Mesozoic theoleites from Antarctica: Geochimica et Cosmochimica Acta, v. 41, p. 15-32.

Griffin, W. L., and Heier, K. S., 1969, Parageneses of garnet in granulite-facies rocks, Lofoten-Vesterålen, Norway: Contributions to Mineralogy and Petrology, v. 23, p. 89-116.

Griffin, W. L., Taylor, P. N., Hakkinen, J. W., Heier, K. S., Iden, I. K., Krogh, E. J., Malm, O., Olsen, K. I., Ormaasen, D. E., and Tveten, E., 1978, Archean and Proterozoic crustal evolution in Lofoten-Vesterålen, north Norway: Journal of the Geological Society of London, v. 135, p. 629-647.

Hakkinen, J. W., 1977, Structural geology and metamorphic history of western Hinnøy and adjacent parts of eastern Hinnøy, north Norway [Ph.D. thesis]: Rice University, Houston, Texas, 161 p.

Hames, W. E., and Andresen, A., 1996, Timing of orogeny and extension in the Continental shelf of north-central Norway as indicated by laser $^{40}Ar/^{39}Ar$ muscovite dating: Geology, v. 24, no. 11, p. 1005-1008.

Harrison, T. M., and Be, K., 1983, $^{40}Ar/^{39}Ar$ age spectrum analysis of detrital microcline from the southern San Joaquin basin, California: An approach to determining the thermal evolution of sedimentary basins: Earth and Planetary Science Letters, v. 64, p. 244-256.

Harrison, T. M., and McDougall, I., 1981, Excess Ar in metamorphic rocks from Broken Hill, New South Wales: implications for $^{40}Ar/^{39}Ar$ age spectra and the thermal history of the region: Earth and Planetary Science Letters, v. 55, p. 123-149.

Harrison, T. M., and McDougall, I., 1982, Thermal signature of potassium feldspar K-Ar ages inferred from $^{40}Ar/^{39}Ar$ age spectrum results: Geochimica et Comsochimica Acta, v. 46, p. 1811-1820.

Heier, K. S., 1960, Petrology and geochemistry of high-grade metamorphic and igneous rocks on Langøy, northern Norway: Norges Geologiske Undersøkelse Bulletin 207, 246 p.

Hodges, K. V., 1982, Tectonic evolution of the Eidsfjord-Sitas Area, Norway-Sweden [Ph.D. thesis]: Massachusetts Institute of Technology, Cambridge, Massachusetts,192 p.

Hodges, K. V., Bartley, J. M., and Burchfiel, B. C., 1982, Structural evolution of an A-type subduction zone, Lofoten-Rombak area, northern Scandinavian Caledonides: Tectonics, v. 1, p. 441-462.

Holloman, J., 1996, Tectonic evolution of a portion of the Lofoten archipelago, Røst, Northern Norway [M.S. thesis]: Auburn University, Auburn, Alabama, 123 p.

Kassos, G., Steltenpohl, M. G., Rehnstrøm, E., Mager, S., and Andresen, A., 2004, Structural and isotopic studies of eclogite-facies shear zones and associated pseudotachylites in lower-crustal continental basement, Lofoten Islands, Norway: Deep-crustal seismic faults?: Geological Society of America Abstracts with

Programs, v. 36, no. 5, p. 430.

Klein, A. C., and Steltenpohl, M. G., 1999, Basement-cover relations and late- to post-Caledonian extension in the Leknes group, west-central Vestvagøy, Lofoten, North Norway: Norsk geologisk tidsskrift, v. 79, p. 19-31.

Klein, A. C., Steltenpohl, M. G., Hames, W. E., and Andresen, A., 1999, Ductile and brittle extension in the southern Lofoten archipelago, north Norway: implications for differences in tectonic style along an ancient collisional margin: American Journal of Science, v. 299, p. 69-89.

Løseth, H., and Tveten, E., 1996, Post-Caledonian structural evolution of the Lofoten and Vesterålen offshore and onshore areas: Norsk geologisk tidsskrift, v. 76, p. 215-230.

Markl, G., 1998, The Eidsfjord anorthosite, Vesterålen, Norway: field observations and geochemical data: Norges Geologiske Undersøkelse Bulletin 434, p. 53-75.

Markl, G., and Bucher, K., 1997, Proterozoic eclogites from the Lofoten islands, northern Norway: Lithos, v. 42, p. 15-35.

Mehnert, K. R., 1968, Migmatites and the origin of granitic rocks, Elsevier Publishing Company, New York, 393 p.

Misra, S. N., and Griffin, W. L., 1972, Geochemistry and metamorphism of dolerite dikes from Austvågøy in Lofoten: Norsk Geologisk Tidsskrift, Supplement, v. 52, p. 409-425.

Mooney, L. J., 1997, Structural and lithologic investigation of Værøy, Lofoten, North Norway and regional study of Caledonian metamorphism [M.S. thesis]: Auburn University, Auburn, Alabama, 108 p.

Olesen, O., Henkel, H., Kjetil, K., and Tveten, E., 1991, Petrophysical properties of a prograde amphibolite-granulite facies transition zone at Sigerfjord, Vesterålen, northern Norway: Tectonophysics, v. 192, p. 33-39.

Olesen, O., Torsvik, T. H., Tveten, E., Zwann, K. B., Løseth, H., and Henningsen, T., 1997, Basement structure of the continental margin in the Lofoten-Lopphavet area, northern Norway: constraints from potential field data, on-land structural mapping and paleomagnetic data: Norsk geologisk tidsskrift, v. 77, p. 15-30.

Plattner, U., Markl, G., and Sherlock, S., 2003, Chemical heterogeneities of Caledonian (?) pseudotachylites in the Eidsfjord anorthosite, north Norway: Contributions to Mineralogy and Petrology, v. 145, p. 316-338.

Purdy, J. W., and Jäger E., 1976, K-Ar ages on rock forming minerals from the central

Alps: Institute of Geology and Mineralogy Memoir, Padova University, v. 30, p. 1-31.

Roberts, D., and Gee, D. G., 1985, An introduction to the structure of the Scandinavian Caledonides, in Gee, D. G., and Sturt, B. A., eds., The Caledonide Orogen - Scandinavia and Related Areas, John Wiley, New York, p. 55-68.

Rykkelid, E., 1992, Contractional and extensional structures in the Caledonides [Dr. Scient. Thesis]: University of Oslo, Oslo, Norway, 178 p.

Scholz, C. H., 1988, The brittle-plastic transition and the depth of seismic faulting: Geologische Rundschau, v. 77, p. 319-329.

Sherlock, S. C., 2001, Two-stage erosion and deposition in a continental margin setting: an $^{40}Ar/^{39}Ar$ laserprobe study of offshore detrital white micas in the Norwegian Sea: Journal of the Geological Society of London, v. 158, p. 793-799.

Sigmond, E. M. O., Gustavson, M., and Roberts, D., 1984, Bergrunnskart over Norge, M., 1:1 million: Norges geologiske undersøkelse.

Spear, F. S., 1993, Metamorphic Phase Equilibria and Pressure-Temperature-Time Paths, Mineralogical Society of America Monograph, Mineralogical Society of America, Washington, D. C., 799 p.

Steltenpohl, M. G., 1987, Tectonostratigraphy and tectonic evolution of the Skånland area, north Norway: Norges Geologisk Undersøkelse, Bulletin 409, p. 1-19.

Steltenpohl, M. G., and Kunk, M. J., 1993, $^{40}Ar/^{39}Ar$ thermochronology and Alleghanian development of the southernmost Appalachian Piedmont, Alabama and southwest Georgia: Geological Society of America Bulletin, v. 105, p. 819-833.

Steltenpohl, M. G., Hames, W. E., and Andresen, A., 2004, The Silurian to Permian history of a metamorphic core complex in Lofoten, northern Scandinavia Caledonides: Tectonics, v. 23, TC1002, doi: 10.1029/2003TC001522.

Steltenpohl, M. G., Hames, W. E., Andresen, A., and Markl, G., 2003, A new Caledonian eclogite province in Norway and potential Laurentian (Taconic) and Baltic links: Geology, v. 31, no. 11, p. 985-988.

Tull, J. F., 1977, Geology and structure of Vestvågøy, Lofoten, north Norway: Norges Geologiske Undersøkelse, v. 333, p. 1-59.

Tull J. F., Bartley, J. M., Hodges, K. V., Andresen, A., Steltenpohl, M. G., and White, J. M., 1985, The Caledonides in the Ofoten region (68-69°N), north Norway: Key aspects of tectonic evolution, in Gee, D. G., and Sturt, B. A., eds., The

Caledonide Orogen - Scandinavia and Related Areas: John Wiley, New York, p. 553-569.

Tullis, J. A., 1983, Deformation of feldspars, in Ribbe, P. H., ed., Feldspar mineralogy: Mineralogical Society of America Short Course Notes, v. 2, p. 297-323.

Waltman, C. K., 1997, Geological investigations into the tectonic evolution of the Scandinavian Caledonides: Lofoten, North Norway [M.S. thesis]: Auburn University, Auburn, Alabama, 111 p.

Zeltner, D. M., 2001, Geological investigations in east Bodø, north-central Norway [M.S. thesis]: Auburn University, Auburn, Alabama, 88 p.

APPENDIX

Tabulated results of the $^{40}Ar/^{39}Ar$ analyses

Sample SM21A Muscovite

J = 0.012284 ± 0.50% smpl wt = 0.0020 g

Temp °C	^{39}Ar (% of total)	^{40}Ar (initial & radiogenic)	^{39}Ar (K-derived)	^{38}Ar (Cl-derived)	^{37}Ar (Ca-derived)	^{36}Ar (initial)	Age (Ma)	1-sigma precision estimates
650	0.4	6.817E-14	2.601E-15	3.009E-16	3.204E-16	***	391.68	± 8.86
750	1.8	2.921E-13	1.210E-14	***	1.935E-16	***	459.28	± 1.61
850	5.3	9.024E-13	3.520E-14	***	3.224E-16	***	490.50	± 0.52
950	39.5	8.358E-12	2.648E-13	8.362E-16	6.893E-16	***	589.48	± 0.21
1000	10.7	2.072E-12	7.142E-14	2.151E-16	6.483E-16	***	548.59	± 0.36
1050	20.7	4.183E-12	1.391E-13	4.362E-16	7.394E-16	***	565.99	± 0.18
1250	21.1	4.472E-12	1.413E-13	4.766E-16	1.881E-15	***	591.12	± 0.22
1450	0.6	1.730E-13	3.758E-15	***	8.791E-16	***	793.00	± 4.11
Total	100.1	2.052E-11	6.703E-13	2.472E-15	5.674E-15	3.067E-16	573.76	

Sample SM127 Muscovite

J = 0.012316 ± 0.50% smpl wt = 0.0019 g

Temp °C	^{39}Ar (% of total)	^{40}Ar (initial & radiogenic)	^{39}Ar (K-derived)	^{38}Ar (Cl-derived)	^{37}Ar (Ca-derived)	^{36}Ar (initial)	Age (Ma)	1-sigma precision estimates
650	0.4	6.903E-14	2.106E-15	1.074E-15	3.238E-16	***	388.13	± 15.65
750	1.5	2.093E-13	7.513E-15	***	5.925E-16	***	522.92	± 2.89
800	1.5	2.081E-13	7.486E-15	***	***	***	523.19	± 3.45
850	3.8	6.178E-13	1.961E-14	***	1.989E-16	***	585.45	± 0.88
900	27.0	4.209E-12	1.379E-13	***	2.583E-16	***	573.19	± 0.24
950	18.7	2.823E-12	9.561E-14	***	3.624E-16	***	557.76	± 0.39
1000	12.1	1.885E-12	6.170E-14	***	3.113E-16	***	573.15	± 0.53
1150	35.0	5.200E-12	1.784E-13	***	5.170E-16	***	551.59	± 0.21
Total	100.0	1.522E-11	5.104E-13	1.284E-15	2.688E-15	3.503E-16	561.05	

Sample SM172 Muscovite

J = 0.012350 ± 0.50% smpl wt = 0.0022 g

Temp °C	^{39}Ar (% of total)	^{40}Ar (initial& radiogenic)	^{39}Ar (K-derived)	^{38}Ar (Cl-derived)	^{37}Ar (Ca-derived)	^{36}Ar (initial)	Age (Ma)	1-sigma precision estimates
850	7.7	9.114E-13	3.468E-14	5.473E-16	5.854E-16	***	501.73	± 0.71
950	37.4	4.609E-12	1.693E-13	9.031E-16	7.587E-16	***	520.77	± 0.31
1050	20.5	2.487E-12	9.269E-14	9.060E-16	8.520E-16	***	514.26	± 0.39
1150	26.3	3.320E-12	1.190E-13	6.550E-16	4.538E-16	***	531.96	± 0.32
1250	8.2	1.111E-12	3.729E-14	2.257E-16	1.018E-15	***	561.84	± 1.01
Total	100.1	1.244E-11	4.530E-13	3.237E-15	3.668E-15	2.263E-16	524.36	

Sample SM92A Muscovite

J = 0.012306 ± 0.50% smpl wt = 0.0020 g

Temp °C	^{39}Ar (% of total)	^{40}Ar (initial & radiogenic)	^{39}Ar (K-derived)	^{38}Ar (Cl-derived)	^{37}Ar (Ca-derived)	^{36}Ar (initial)	Age (Ma)	1-sigma precision estimates
550	0.3	2.152E-13	2.168E-15	6.529E-16	2.364E-16	5.862E-16	385.90	± 8.83
650	0.4	6.214E-14	3.005E-15	4.350E-16	2.815E-16	***	319.96	± 8.09
750	1.3	2.118E-13	9.412E-15	3.990E-16	2.142E-16	***	434.21	± 1.93
850	5.0	7.855E-13	3.635E-14	6.937E-16	3.103E-16	***	421.23	± 0.74
950	45.0	7.512E-12	3.253E-13	1.602E-15	1.287E-15	***	449.85	± 0.16
1050	14.4	2.430E-12	1.039E-13	1.433E-15	3.398E-16	***	454.37	± 0.31
1150	30.5	4.601E-12	2.204E-13	8.669E-16	3.533E-16	***	411.82	± 0.20
1250	2.8	4.630E-13	2.045E-14	***	2.606E-16	***	440.59	± 1.05
1450	0.3	1.085E-13	1.995E-15	***	***	***	890.56	± 7.32
Total	100.0	1.639E-11	7.231E-13	6.216E-15	3.385E-15	8.520E-16	437.76	

Sample HU2 Muscovite

J = 0.012309 ± 0.50% smpl wt = 0.0022 g

Temp °C	^{39}Ar (% of total)	^{40}Ar (initial & radiogenic)	^{39}Ar (K-derived)	^{38}Ar (Cl-derived)	^{37}Ar (Ca-derived)	^{36}Ar (initial)	Age (Ma)	1-sigma precision estimates
550	0.2	1.862E-13	1.891E-15	5.699E-16	2.848E-16	5.563E-16	239.52	± 20.34
650	0.3	7.085E-14	2.681E-15	***	2.175E-16	***	398.78	± 13.41
750	1.6	3.264E-13	1.335E-14	***	2.112E-16	***	454.14	± 2.09
850	7.5	1.533E-12	6.198E-14	***	4.408E-16	***	468.60	± 0.58
950	46.7	9.107E-12	3.851E-13	3.753E-16	6.624E-16	2.230E-16	458.10	± 0.18
1050	35.1	6.804E-12	2.896E-13	2.845E-16	8.972E-16	1.475E-16	455.64	± 0.19
1100	3.0	5.821E-13	2.460E-14	***	3.508E-16	***	457.70	± 1.22
1150	1.4	2.676E-13	1.121E-14	***	1.598E-16	***	451.83	± 2.84
1200	1.1	2.260E-13	9.365E-15	***	2.678E-16	***	459.22	± 3.29
1250	0.9	1.890E-13	7.796E-15	***	3.422E-16	***	458.88	± 5.01
1350	1.1	2.218E-13	9.375E-15	***	2.563E-16	***	448.81	± 4.26
1450	0.9	1.733E-13	7.077E-15	***	***	***	453.17	± 4.25
Total	99.8	1.969E-11	8.240E-13	1.732E-15	4.194E-15	1.307E-15	457.04	

Sample SM135B Muscovite

J = 0.012309 ± 0.50% smpl wt = 0.0019 g

Temp °C	^{39}Ar (% of total)	^{40}Ar (initial & radiogenic)	^{39}Ar (K-derived)	^{38}Ar (Cl-derived)	^{37}Ar (Ca-derived)	^{36}Ar (initial)	Age (Ma)	1-sigma precision estimates
750	0.9	1.934E-13	7.832E-15	***	1.620E-16	***	460.16	± 2.31
800	1.5	3.149E-13	1.295E-14	***	2.008E-16	***	462.54	± 1.90
850	2.5	5.559E-13	2.244E-14	***	2.393E-16	***	472.46	± 1.52
900	16.7	3.872E-12	1.483E-13	1.573E-16	3.170E-16	***	497.92	± 0.20
950	29.5	6.790E-12	2.610E-13	3.108E-16	6.899E-16	***	498.90	± 0.14
1000	8.3	1.941E-12	7.391E-14	***	2.232E-16	***	501.96	± 0.34
1100	38.8	9.036E-12	3.436E-13	3.204E-16	9.122E-16	***	504.30	± 0.14
1150	1.0	2.431E-13	9.101E-15	***	2.835E-16	***	507.66	± 3.00
1350	0.7	1.815E-13	6.539E-15	***	8.893E-16	***	510.84	± 4.14
Total	99.9	2.313E-11	8.857E-13	1.130E-15	3.917E-15	5.410E-16	499.74	

Sample SM135B Potassium Feldspar

J = 0.012320 ± 0.50% smpl wt = 0.0020 g

Temp °C	^{39}Ar (% of total)	^{40}Ar (initial & radiogenic)	^{39}Ar (K-derived)	^{38}Ar (Cl-derived)	^{37}Ar (Ca-derived)	^{36}Ar (initial)	Age (Ma)	1-sigma precision estimates
750	4.5	4.537E-13	4.018E-14	***	2.844E-16	***	232.12	± 0.87
850	16.4	1.689E-12	1.474E-13	***	6.142E-16	***	237.65	± 0.26
950	22.1	2.417E-12	1.987E-13	***	1.683E-15	***	251.24	± 0.22
1050	11.9	1.610E-12	1.068E-13	***	1.112E-15	***	305.52	± 0.38
1150	4.7	7.952E-13	4.236E-14	***	6.658E-16	***	371.33	± 1.29
1250	17.4	3.714E-12	1.562E-13	***	2.384E-15	***	460.11	± 0.24
1350	23.0	4.796E-12	2.070E-13	***	7.740E-16	***	449.99	± 0.41
Total	100.0	1.548E-11	8.986E-13	2.177E-16	7.517E-15	3.547E-16	344.98	

Sample HU2 Potassium Feldspar

J = 0.012276 ± 0.50% smpl wt = 0.0020 g

Temp °C	^{39}Ar (% of total)	^{40}Ar (initial & radiogenic)	^{39}Ar (K-derived)	^{38}Ar (Cl-derived)	^{37}Ar (Ca-derived)	^{36}Ar (initial)	Age (Ma)	1-sigma precision estimates
650	2.7	1.754E-10	1.814E-14	2.126E-16	2.233E-16	***	175.24	± 2.21
750	6.9	4.026E-13	4.572E-14	***	3.943E-16	***	182.39	± 0.81
850	8.6	6.059E-13	5.715E-14	***	6.022E-16	***	219.37	± 0.65
950	7.4	6.053E-13	4.910E-14	***	7.431E-16	***	251.83	± 0.84
1050	7.4	8.046E-13	4.892E-14	***	8.090E-16	***	327.95	± 0.60
1150	3.2	4.202E-13	2.145E-14	***	3.699E-16	***	380.26	± 1.33
1250	14.1	2.195E-12	9.387E-14	1.620E-16	3.400E-15	3.099E-16	438.46	± 0.42
1350	36.4	4.693E-12	2.420E-13	2.718E-16	3.325E-15	5.290E-16	373.61	± 0.15
1450	8.4	1.103E-12	5.569E-14	***	8.345E-16	***	380.79	± 0.52
1650	5.0	6.118E-13	3.324E-14	***	4.403E-16	***	348.77	± 0.81
Total	100.1	1.162E-11	6.653E-13	8.795E-16	1.114E-14	1.287E-15	339.90	

Sample Q Potassium Feldspar

J = 0.012267 ± 0.50% smpl wt = 0.0020 g

Temp °C	^{39}Ar (% of total)	^{40}Ar (initial & radiogenic)	^{39}Ar (K-derived)	^{38}Ar (Cl-derived)	^{37}Ar (Ca-derived)	^{36}Ar (initial)	Age (Ma)	1-sigma precision estimates
650	2.5	3.167E-13	2.873E-14	2.239E-16	6.281E-16	***	206.59	± 1.19
750	3.7	4.730E-13	4.349E-14	***	6.081E-16	***	220.22	± 0.73
800	2.0	2.414E-13	2.342E-14	***	3.837E-16	***	209.82	± 1.71
850	1.7	2.112E-13	2.011E-14	***	5.419E-16	***	211.64	± 1.32
900	1.6	1.898E-13	1.841E-14	***	2.699E-16	***	208.99	± 1.49
950	1.8	2.126E-13	2.032E-14	***	4.036E-16	***	213.18	± 2.17
1000	2.0	2.475E-13	2.312E-14	***	4.678E-16	***	217.91	± 1.18
1100	4.9	6.122E-13	5.636E-14	***	4.973E-16	***	220.23	± 0.59
1150	5.3	6.803E-13	6.153E-14	***	8.250E-16	***	220.25	± 0.42
1350	63.4	8.605E-12	7.364E-13	1.088E-15	3.527E-15	8.936E-16	234.70	± 0.04
1650	11.1	1.554E-12	1.290E-13	2.034E-16	7.640E-16	2.017E-16	239.73	± 0.40
Total	100.0	1.334E-11	1.161E-12	1.879E-15	8.916E-15	1.496E-15	230.55	